JGR Earth Surface

RESEARCH ARTICLE
10.1029/2023JF007342

Special Section:
Controls and Biasing Factors in Sediment Generation, Routing, and Provenance: Models, Methods, and Case Studies

The Zircon Story of the Niger River: Time-Structure Maps of the West African Craton and Discontinuous Propagation of Provenance Signals Across a Disconnected Sediment-Routing System

Guido Pastore[1], Eduardo Garzanti[1], Pieter Vermeesch[2], Germain Bayon[3], Alberto Resentini[1], Nadine Braquet[4], and Brume Overare[5,6]

[1]Laboratory for Provenance Studies, Department of Earth and Environmental Sciences, University of Milano-Bicocca, Milano, Italy, [2]London Geochronology Centre, Department of Earth Sciences, University College London, London, UK, [3]Unité de Recherche Geosciences Marines, Ifremer, Plouzané, France, [4]Institut de Recherche pour le Développement IRD – UMR G-eau INRAE, Montpellier, France, [5]Department of Earth Sciences, Memorial University of Newfoundland, St. John's, NL, Canada, [6]Department of Earth Sciences, Federal University of Petroleum Resources, Effurun, Nigeria

Abstract The Niger River drains a large part of the West African Craton, where rocks ranging in age from Paleoarchean to recent offer an unexcelled opportunity to map the diverse time structures of sediment sources and provide essential information for provenance diagnoses. In this study, U-Pb zircon dating is complemented with bulk-sand geochemical (Zr, Hf, REE) and Nd-Hf isotope data to pin-point parent rocks of zircon grains and draw inferences on sediment generation across sub-Saharan western Africa. In Upper Niger sand, zircon ages pass from exclusively Archean in Guinea headwaters to dominantly Paleoproterozoic in the Inner Delta in Mali, testifying to the progressive dilution by tributary sediment derived from the Birimian domain. Zircon ages abruptly change to dominantly Neoproterozoic downstream of the Inner Delta, becoming indistinguishable from those in Saharan eolian dunes across the Sahel. Most of the sediment generated in the headwaters is thus dumped in the marshlands and bedload is reconstituted downstream by recycling eolian sand. Zircon grains in the Lower Niger yielded virtually the same U-Pb ages as in Benue sediment, indicating an overwhelming supply from the Benue tributary. In the Niger Delta, however, Archean zircons reappear, and both ε_{Nd} and ε_{Hf} values become notably more negative, indicating extensive reworking of sand deposited along the coastal plain at earlier times of wetter climate, when artificial barriers to the sediment flux did not exist in the upper to middle Niger River catchment.

Plain Language Summary Across sub-Saharan western Africa, the Niger River drains rocks with ages spanning more than 3 billion years. In such a vast region, diverse techniques can be combined to identify processes of erosion and transport, starting from the analysis of sediments and the zircon grains they contain. The very old ages of zircons derived from Guinean headwaters (all older than 2650 million years) are gradually diluted by younger zircons generated in SW Mali (from 1900 to 2200 million years), whereas a sharp change to more recent zircon ages (from 500 to 700 million years) is documented downstream of the Inner Delta. Most sediment generated in the headwaters is thus dumped in these marshlands and subsequently replaced with sand eroded from eolian dunes along the southern edge of the Sahara Desert. Rigid segmentation of fluvial sediment transport has become the rule after the extensive construction of dams worldwide, but can also be caused by natural processes. Marshlands formed at the subequatorial edge of tropical deserts can represent very efficient natural barriers to sediment transport, preventing a large part of the detritus generated in the highlands from reaching the ocean, with consequent impact on both sediment budgets and sediment composition.

Key Points:

- The Niger River offers an unexcelled opportunity to use detrital geochronology to map the diverse time structures of sediment sources
- Sand generated in the headwaters is dumped in the Inner Delta as indicated by a significant change in the U-Pb signature and ε_{Nd}-ε_{Hf} values
- Reworking of sand along the coastal plain testifies the absence of artificial or major natural barriers to the sediment flux in earlier times

Supporting Information:

Supporting Information may be found in the online version of this article.

Correspondence to:

G. Pastore and E. Garzanti,
g.pastore2@campus.unimib.it;
eduardo.garzanti@unimib.it

Citation:

Pastore, G., Garzanti, E., Vermeesch, P., Bayon, G., Resentini, A., Braquet, N., & Overare, B. (2023). The zircon story of the Niger River: Time-structure maps of the West African Craton and discontinuous propagation of provenance signals across a disconnected sediment-routing system. *Journal of Geophysical Research: Earth Surface*, *128*, e2023JF007342. https://doi.org/10.1029/2023JF007342

Received 15 JUL 2023
Accepted 23 OCT 2023

1. Introduction

Detrital-zircon geochronology has been so extensively used in the last decade that it can be considered to have ushered in a new era in provenance analysis. Detrital geochronology provides an additional dimension to petrographic data, which is per se unable to determine whether igneous or metamorphic rocks exposed in source terranes are young or old, and hence whether those terranes are active orogenic belts or ancient orogenic roots exposed along rift shoulders or at the core of a craton (Garzanti, 2016).

However, detrital-zircon geochronology is not the only tool to determine the age of source terranes and the limitations of the method are considerable. Zircon grains typically account for only a tiny fraction (<0.05%) of bulk sand, and sand in rivers is transported as bedload, which generally represents only a minor fraction of the total sediment flux (<10%; Hay, 1998). Being one of the most durable minerals, and consequently largely derived from recycling of older siliciclastic rocks in most sedimentary basins, zircon ages do not necessarily reflect the age of the source rocks but largely that of the primary magmatic or metamorphic rocks in which zircon originally crystallized (protosources of Pell et al. (1997)).

More geochronological tools exist, including U-Pb dating of other detrital minerals (e.g., rutile, apatite, or titanite), $^{40}Ar/^{39}Ar$ dating of detrital mica, fission-track dating of apatite or zircon itself, each of which highlights a different age characteristic (time structure) of source rocks (e.g., Guo et al., 2020; Najman, 2006; von Eynatten & Dunkl, 2012). Additionally, model mantle extraction ages can be calculated by the analysis of isotopic parent-daughter tracers such as Sm-Nd or Lu-Hf (e.g., Bea et al., 2018; DePaolo et al., 1991; Vervoort et al., 1999). A variety of age maps of source areas can thus be produced by the determination of isotopic ratios in sediments (Goldstein et al., 1997; Padoan et al., 2011).

Especially in a geologically understudied region such as subequatorial Africa, detrital geochronology allows us to obtain a wider and more representative overview of a large river catchment than bedrock data (D. Burbank in Greensfelder (2002)), to identify sources overlooked by bedrock geochronology, and to assess the relative importance of crustal-growth episodes provided that mineral fertility and erosion rates in different source-rock domains are taken into due account (Chew et al., 2020; Malusà et al., 2016; Samson et al., 2018).

The Niger River catchment encompasses a large part of cratonic sub-Saharan western Africa, where metamorphic and igneous rocks range from the Paleoarchean granitoid gneisses of the Man Shield in Guinea to the recent anorogenic lavas of the Cameroon Line (Figure 1). Such a great variety in the age of source rocks offers an unexcelled opportunity to test the validity of detrital-zircon geochronology as a provenance tracer and to highlight the complexities of segmented sediment-transport systems (Caracciolo, 2020; Garzanti, Bayon, Dinis, et al., 2022; Hinderer, 2012).

This study uses different isotopic tracers, primarily U-Pb detrital-zircon ages complemented by bulk-sediment Nd and Hf isotope data, to integrate the available literature information on the age structure of rocks exposed across a large part of the West African Craton, an extensive compilation of which is provided in the Appendix S3 in Supporting Information S1. The new data allow us to monitor the discontinuous propagation of provenance signals along the Niger River, here divided for convenience into four tracts: the Upper Niger from the headwaters in Guinea to the Inner Delta in Mali, the Sahelian Niger from the Inner Delta to the Nigerian border (which roughly corresponds to the southern limit of the Sahel region), the Middle Niger upstream of the Benue confluence, and the Lower Niger downstream (Figure 1). Specifically, we document the disconnection of sediment transport across the Inner Delta in Mali, the reconstitution of sediment load by reworking of Saharan dunes across the Sahel, and the prominent sediment contribution from the Benue River in Nigeria.

2. The Niger River

The Niger River (length ~4.200 km, basin area 2,100,000 km^2), the third largest in Africa and the twelfth longest on Earth (Welcomme & Dumont, 1986), rises at an altitude of ~800 m, only 250 km east of the Atlantic coast in hot-wet subequatorial Guinea. In Mali, after entering the semi-arid Sahel zone in Taoudeni Basin lowlands covered by eolian dunes at the edge of the Sahara Desert, the Niger River and its Bani tributary (length 1,100 km, basin area ~130,000 km^2) form the Inner Delta, a wide wetland area where two-thirds of the flow is lost owing to seepage and evaporation (Olivry et al., 1994; Picouet et al., 2002; Zaré et al., 2017).

2.1. Water and Sediment Fluxes

In the Upper Niger catchment, precipitation is concentrated in summer and decreases steadily from over 2 m/a in subequatorial Guinea to 0.15–0.4 m/a in the Inner Delta and even less in the Sahara Desert to the north (L'Hôte & Mahé, 1995). Rainfall increases steadily southwards in Nigeria, from 0.5 to 0.75 m/a in the Sahel to 2 m/a and more along the coast where the wet season lasts from March to October. The annual river flood occurs in different months across the basin (Ferry et al., 2012). In the Upper Niger, discharge is high in the rainy summer and low in the dry winter, but the flow slows down sharply across the very-low gradient and wide flooded area of the Inner Delta (Olivry et al., 1995). This *black flood* from upstream, characterized by clear desilted waters, thus crosses the

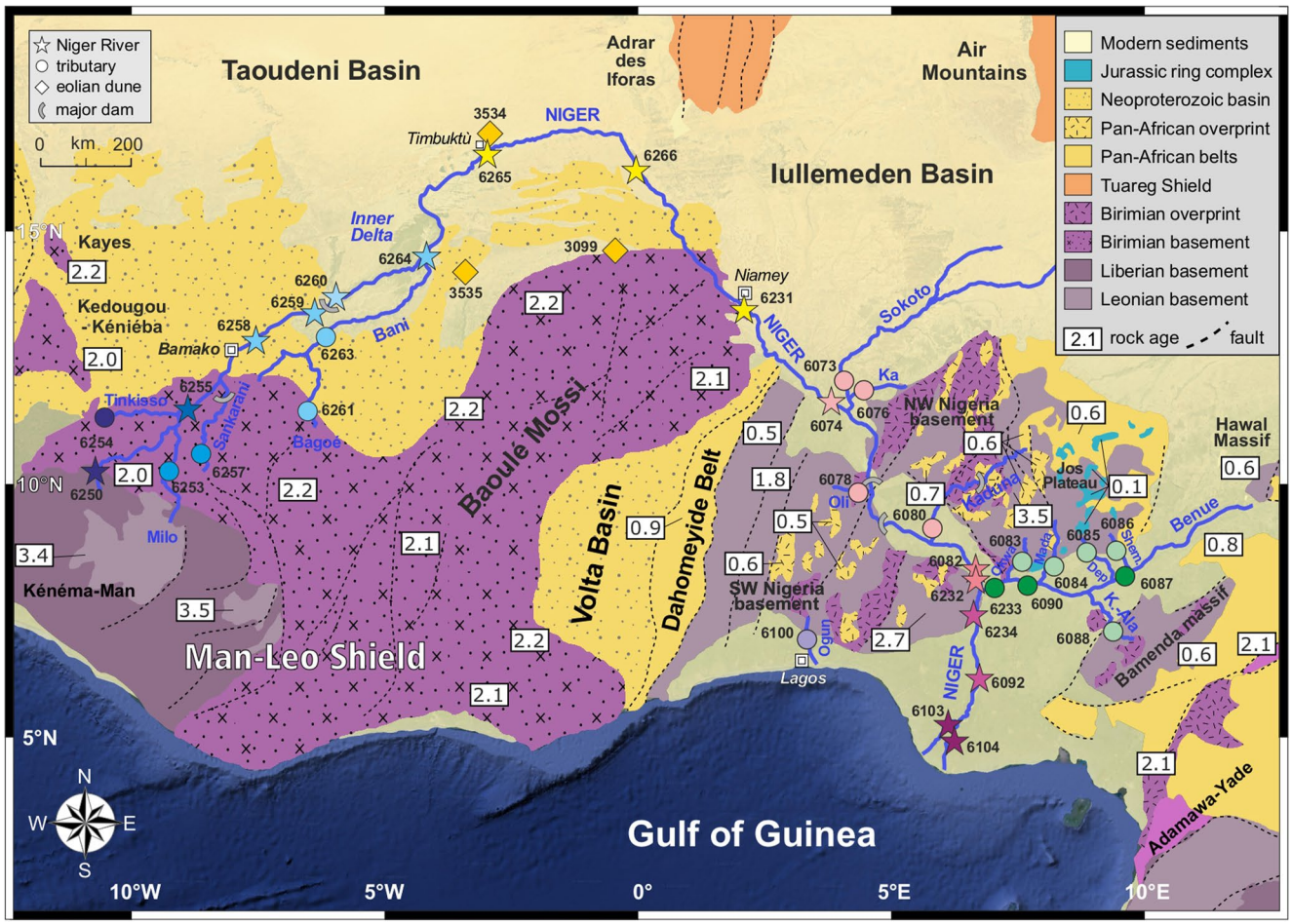

Figure 1. The Niger River in southern West Africa. The main geological domains and their bedrock age signatures are indicated, together with sampling sites and sample numbers. The Adrar des Iforas, Air Mountains, and Nigeria and Cameroon basements are all part of the Pan-African Trans-Saharan Belt, which binds the West African, Saharan, and Congo cratons (Caby, 1987; Ferré et al., 2002).

Sahelian Niger only in winter, reaching the Middle Niger well after the *white flood* characterized by waters laden with kaolinitic sediments that shortly follows the local summer rain season (Ogunkoya, 2023). The Benue River, instead, has only one flood season between May and October. Consequently, discharge in the Lower Niger peaks in November, with a slight rise in winter caused by floodwaters from the Upper Niger. The water budget remains negative across the Sahel from Mali to Niger, and the annual flow entering Nigeria has decreased considerably in the last decades. The water flux is restored across Nigeria, where large contributions from tributaries, including the Kaduna (length 575 km, basin area ~66,000 km^2) and especially the Benue (length 1,400 km, basin area ~340,000 km^2), fuel an average water discharge of ~270 km^3/year at the Niger Delta (FAO & IHE Delft, 2020).

The suspended sediment and dissolved loads for the entire Niger River were estimated as ~40 and ~10 million tons/a, respectively (Hay, 1998; Milliman & Farnsworth, 2011). Based on gauged data (NEDECO, 1961), annual bedload and suspended load were assessed to be 0.3 and 4.6 million tons for the Middle Niger and 0.6 and 11 million tons for the Benue River, respectively (Adegoke et al., 2017). Middle Niger load has been reduced by impoundment in major artificial reservoirs, including Kainji Lake in western Nigeria (dam completed in 1968), the hydropower Jebba Dam ~100 km downstream (completed in 1984; Yue et al., 2022), and the Shiroro Dam on the Kaduna tributary ~230 km upstream of the confluence with the Niger River (completed in 1990; Daramola et al., 2022). The ~450 km-long Lower Niger forms the largest delta in Africa (~19,000 km^2), characterized by high distributary density and extensive development of tidal flats and freshwater marshes (Allen, 1965; Coleman et al., 2008; Kuenzer et al., 2014). The wave-modeled lobate shoreline reflects high nearshore wave action and sediment transport by divergent bi-directional longshore currents (Anthony, 2015).

2.2. Geology of the Niger Catchment

The Niger River cuts across the southern part of the West African Craton, welded during the Eburnean (Birimian) orogeny around 2.1 Ga. Archean rocks represent the core of the Man Shield in Guinea, the basement of the Taoudeni basin in Mali, and the core of the Nigeria basement complex (Figure 1).

The Man Shield, drained by Niger headwater branches, contains partially retrogressed amphibolite-to granulite-facies Paleoarchean and Mesoarchean rocks of the Kénéma-Man domain. The oldest ages were obtained from eclogite xenoliths (3.4 Ga) and zircon cores within tonalitic gneisses (~3.6 Ga; Barth et al., 2002). The shield, comprising upper Mesoarchean (Leonian: 3.0–2.9 Ga) to lower Neoarchean (Liberian: 2.8–2.7 Ga) plutonic rocks and supracrustal intercalations including banded iron formations containing Liberian zircons (Thiéblemont et al., 2001, 2004), is rimmed by a belt of granodiorites and subordinate monzogranites and granites with arc-like geochemical signatures emplaced at 2.05–2.07 Ga (Egal et al., 2002).

Instead, the Baoulé and Bagoé headwater branches of the Bani River drain the Paleoproterozoic Baoulé-Mossi (Birimian) domain to the east, which includes Rhyacian igneous and metamorphic rocks and the Siguiri Basin drained by the Niger River in the west. Volcanic activity began at ~2.2 Ga in the east and shifted westward until ~2.06 Ga (Grenholm et al., 2019; Lahondère et al., 2002). Early intrusives are dated at 2.27–2.23 Ga (Parra-Avila et al., 2017), with main pulses at 2.19–2.08 Ga (Kristindóttir et al., 2013). Zircon grains in modern sand of small Niger and Bani tributaries yielded an age peak at ~2.1 Ga and a minor cluster between 2.2 and 2.35 Ga (Parra-Avila et al., 2016). The Birimian Siguiri Basin comprises siliciclastic strata intercalated with lava and pyroclastic rocks with subduction-zone geochemical affinity dated as 2.2–2.1 Ga (Lahondère et al., 2002; Lebrun et al., 2016). Amphibolite-facies micaschists and calcsilicate rocks occur close to granitoid intrusions (Egal et al., 2002; Lerouge et al., 2004). The overlying Neoproterozoic-Cambrian siliciclastic strata, with a basal tillite deposited during the late Cryogenian Marinoan glaciation (Deynoux et al., 2006), are widely exposed along the southern margin of the Taoudeni Basin (Figure 1). Lower Jurassic dolerites emplaced during rifting of the central Atlantic Ocean also sparsely occur in the west (Deckart et al., 2005).

After drawing a great arc across the southern edge of the Sahara Desert, the Niger River in Niger flows between the edge of the Paleoproterozoic Birimian rocks of the Leo Shield in the west, widely exposed in Burkina Faso and including medium-high grade gneiss and migmatite granite, and the Neoproterozoic covers and Cenozoic sediments of the Iullemeden-Sokoto Basin encircled by Cretaceous epicontinental marine deposits in the east (Figure 1). Downstream, the Niger River flows along the northernmost margin of the Dahomeyide Belt, accreted in the Neoproterozoic during the collision between the West African Craton and the Nigerian Shield (Affaton et al., 1991; Attoh et al., 1997; Caby, 1987). Gneisses, metagabbros and metadiorites mostly yielded Neoproterozoic ages clustering between 650 and 550 Ma (Affaton et al., 2000; Kalsbeek et al., 2012), but Paleoproterozoic gneisses dated as ~2.1 Ga also occur (Ganade et al., 2016; Glodji, 2012).

In Nigeria, the Middle Niger flows along the Bida Basin (Rahaman et al., 2019) as the Benue River flows along the Benue Trough (Abubakar, 2014), both being failed arms of the Cretaceous rift system associated with the opening of the northern South Atlantic Ocean (Burke et al., 1971; Fairhead et al., 2013; Obaje et al., 2020). The Bida rift trough separates the SW Nigeria basement, drained by the Oli tributary of the Niger River and by the Ogun River draining directly into the Gulf of Guinea, from the NW Nigeria basement, drained by the Ka and Kaduna tributaries of the Niger River. The Benue rift trough separates the eastern part of the North Nigeria basement drained by the Okwa, Mada, Dep (Ankwe), and Shemanker tributaries of the Benue River from the Bamenda Massif in the southeast, drained by the Katsina-Ala tributary (Figure 1).

The Nigeria basement comprises a Mesoarchean migmatite-gneiss complex and Proterozoic schist belts. The cratonic core, including orthogneisses as old as 3.6 Ga (Kröner et al., 2001) and 3.05 Ga (Bruguier et al., 1994), underwent multistage crustal growth and reworking in the Neoarchean (2.7 and 2.5 Ga; Oversby, 1975; Pidgeon et al., 1976) and in the Paleoproterozoic (2.3–1.8; Rahaman, 1988). The NW Nigeria basement (Fitches et al., 1985) and eastern part of the SW Nigeria basement (Caby & Boesse, 2001; Zeh & Holness, 2003) comprise both polymetamorphic rocks and remnants of cover sequences reaching greenschist-facies to amphibolite-facies and locally including banded iron formations, basalts, siliciclastic rocks, and carbonates (Turner, 1983).

After a prolonged period of quiescence, the Nigeria basement was intruded by Neoproterozoic granites (825–500 Ma; "Older granites") during collision and welding of the West African Craton with Congo and East Saharan cratonic blocks along the Trans-Saharan Belt (Ferré et al., 2002; Ominigbo, 2022; Toteu et al., 2004). In the North Nigeria basement, granites were mainly intruded between 710 and 500 Ma (Elatikpo et al., 2022 and references therein)

but Tonian (825–764 Ma) intrusive rocks also occur locally (Goodenough et al., 2014; Ogezi, 1977). Granitoid intrusions of similar ages occur in the SW Nigeria basement (715–580 Ma; Ferré et al., 1996; Tubosun et al., 1984).

The Bamenda Massif, part of the Adamawa-Yadé province at the north-western edge of the Cameroon basement, largely consists of plutonic (granodiorite, biotite granite) and metamorphic rocks (garnet micaschist, orthogneiss, migmatite; Ibe, 2020; Ominigbo et al., 2020). This Paleoproterozoic core (2.5–2.1 Ga; Penaye et al., 1989; Soba et al., 1991) was reworked and intruded at 832–545 Ma (Bouyo et al., 2015 and references therein). Upper Neoproterozoic granitoids are common in the Hawal Massif to the northeast (595–580 Ma; Bute et al., 2020; Dawai et al., 2013; Ngoniri et al., 2021).

Ring complexes comprising alkali-feldspar granites of mostly Jurassic age (190–145 Ma; "Younger granites"; Obaje, 2009), associated with rhyolite and minor gabbro and syenite, occur in the Jos Plateau in the eastern part of the North Nigeria basement (Bowden & Kinnaird, 1984; Ngako et al., 2006). Ring complexes display a southward-younging trend, with the oldest intrusions dated as ~330 Ma in the north (Rahaman et al., 1984; Vincent et al., 2022). The volcanic activity is documented by the intrusion of trachyte-phonolite plugs in the Benue Trough during the Miocene (22–11 Ma), followed by widespread eruption of basaltic lava since 7 Ma (Grant et al., 1972).

3. Methods

Thirty-four samples of river sand were collected from active fluvial bars through the entire Niger catchment, 11 in the headwaters in Guinea and Mali in June to early July 2022 (six from the mainstem, five from major tributaries), three from the mainstem across the Sahel in Mali and Niger, eight from the Middle Niger (four each from the mainstem and tributaries), seven from the Benue (three from the mainstem, five from tributaries), four from the Lower Niger and distributaries in the Niger Delta, and one from the Ogun coastal river. Data from three samples collected from Saharan dunes on both sides of the Niger course, illustrated in Pastore et al. (2021), were also considered. Full information on sampling sites is provided in Appendix S1 in Supporting Information S1 and Google Earth® file *NigerDZ.kmz*.

3.1. Petrography, Heavy Minerals, Geochemistry

Petrographic analyses were carried out by counting 450 points in each thin section of bulk-sand samples using the Gazzi-Dickinson method (Ingersoll et al., 1984). Sand was classified according to the three main groups of framework components (Q, quartz; F, feldspars; L, lithic fragments), considered if exceeding 10%QFL and listed in order of abundance (classification scheme of Garzanti (2019)). Heavy-mineral analyses were conducted by point counting of ~200 transparent minerals with density >2.90 g/cm^3 on grain mounts of the 15–500 μm fraction obtained by wet sieving of sand samples (Garzanti & Andò, 2019). The equivalent diameter (d_e) was determined by image analysis as the geometric mean of the long and short axes of each zircon grain identified in the studied samples by semi-automatic Raman spectroscopy. The mean size (in ϕ units), sorting ($\sigma\phi$), and skewness (Sk) of the d_e distribution were calculated following Folk and Ward (1957).

The concentration of trace elements including Zr, Hf, and REEs was measured on the powdered 63–2,000 μm class of sand samples digested by alkaline fusion with a Thermo Scientific Element XR sector field ICP-MS at the Pôle Spectrométrie Océan (Bayon et al., 2009). Neodymium and hafnium isotopes were measured using a Thermo Scientific Neptune multi-collector ICP-MS after Nd and Hf purification by conventional ion chromatography (Chu et al., 2002). Repeated analyses of a JNdi-1 standard solution gave $^{143}Nd/^{144}Nd = 0.512116 \pm 0.000012$ (2σ, $n = 19$), in agreement with the recommended value of 0.512115 (Tanaka et al., 2000) and corresponding to an external reproducibility of ±0.22 ε (2σ). Epsilon Nd values were calculated using the present-day chondritic (CHUR) values $^{143}Nd/^{144}Nd = 0.512630$ and $^{147}Sm/^{144}Nd = 0.196$ (Bouvier et al., 2008). Neodymium depleted mantle model ages ($T_{Nd,DM}$) were calculated following De Paolo (1981) and using measured Sm and Nd concentrations ($^{147}Sm/^{144}Nd = Sm/Nd \times 0.6049$) and present-day depleted mantle values of $^{143}Nd/^{144}Nd = 0.513073$ and $^{147}Sm/^{144}Nd = 0.21083$ (Garçon, 2021).

Mass-bias corrections were made using the exponential law, using $^{179}Hf/^{177}Hf = 0.7325$. Repeated analyses of the JMC-475 standard solution gave $^{176}Hf/^{177}Hf = 0.282161 \pm 0.000007$ (2σ, $n = 10$), in agreement with the recommended value of 0.282163 (Blichert-Toft et al., 1997) and corresponding to an external reproducibility of ±0.23 ε (2σ). Epsilon Hf values were calculated using the present-day chondritic (CHUR) values $^{176}Hf/^{177}Hf = 0.282785$ and $^{176}Lu/^{177}Hf = 0.03360$ (Bouvier et al., 2008). Hafnium depleted mantle model ages ($T_{Hf,DM}$) were calculated using measured Lu and Hf concentrations ($^{176}Lu/^{177}Hf = Lu/Hf \times 0.142$) and present-day depleted mantle values of $^{176}Hf/^{177}Hf = 0.283294$ and $^{176}Lu/^{177}Hf = 0.03933$ (Blichert-Toft & Puchtel, 2010).

Key mineralogical and geochemical parameters are summarized in Table 1; the complete petrographic, heavy-mineral, geochemical, and zircon-size data sets are provided in Appendix S1 in Supporting Information S1.

Table 1
Key Petrographic, Heavy-Mineral, and Geochemical Parameters

River	Sample	GSZ (μm)	Q (%)	KF (%)	P (%)	L (%)	tHMC (%)	Zrn (%)	Tur (%)	TiOx (%)	Ep (%)	Grt (%)	SAKS (%)	Amp (%)	Px (%)	&tHM (%)	Zr (ppm)	Hf (ppm)	Nd (ppm)	ε_{Nd}	$T_{Nd,CHUR}$ (Ma)	$T_{Nd,DM}$ (Ma)	ε_{Hf}	$T_{Hf,CHUR}$ (Ma)	$T_{Hf,DM}$ (Ma)
Niger @ Faranah	6250	100	66	30	5	0	1.2	28	1	3	40	0	0	26	0	0	692	16.5	7.7	−41.0	3,529	3,667	−66.5	2,994	3,230
Tinkisso	6254	221	66	26	7	0	1.2	30	1	5	30	0	0	26	8	0	1,428	35.7	8.3	−29.7	2,519	2,797	−49.1	2,229	2,583
Milo	6253	110	73	16	11	0	1.1	10	1	2	36	0	3	46	1	0	346	9.1	4.2	−29.3	3,197	3,422	−52.1	2,620	2,941
Niger @ Dialakoro	6255	150	83	11	6	0	0.8	22	7	5	13	0	3	46	2	0	801	20.5	11.8	−36.2	3,150	3,343	−58.9	2,660	2,948
Sankarani	6257	405	83	12	4	0	2.0	13	7	2	25	0	4	47	0	1	529	12.5	7.5	−29.4	2,482	2,764	−47.2	2,173	2,540
Niger @ Koulikoro	6258	480	93	4	3	0	0.2	24	13	8	16	0	10	23	6	1	95	2.0	2.9	−23.4	2,265	2,616	−53.8	2,594	2,908
Niger @ Ségou	6259	500	92	7	1	0	0.1	14	14	2	8	0	19	34	8	2	77	1.6	5.0	−21.8	2,010	2,384	−49.1	2,455	2,802
Niger @ Markala	6260	130	95	4	1	1	0.6	47	12	11	5	0	10	13	0	2	846	21.8	5.9	−31.2	2,588	2,851	−54.7	2,479	2,794
Bagoé	6261	517	93	4	3	0	0.5	26	35	11	7	1	5	12	3	0	313	7.7	13.9	−18.8	1,538	1,940	−38.5	1,830	2,261
Bani	6263	280	94	5	1	0	0.5	38	23	25	2	0	9	1	0	2	98	2.3	3.1	−18.5	1,995	2,424	−37.8	1,904	2,344
Inner Delta	6264	350	96	4	0	0	0.1	28	20	3	9	0	23	17	1	0	66	1.3	5.3	−23.2	1,975	2,330	−42.5	2,170	2,571
Niger @ Timbuktú	6265	240	99	0	1	0	0.2	47	36	6	6	0	2	2	0	0	95	1.7	4.8	−15.0	1,466	1,944	−25.8	1,300	1,841
Niger @ Gao	6266	230	98	1	1	1	0.3	38	17	13	15	2	5	10	0	2	79	1.5	4.9	n.d.	n.d.	n.d.	−21.9	978	1,515
Komokani dune	3535	165	100	0	0	0	0.1	45	35	12	1	0	6	0	0	1	60	1.0	2.5	−11.7	940	1,416	−34.5	1,820	2,291
Timbuktú dune	3534	215	100	0	0	0	0.1	40	41	10	5	1	1	0	0	0	66	1.1	2.5	−12.7	1,101	1,586	−35.7	1,863	2,324
Oursi dune	3099	255	100	0	0	0	0.2	55	18	4	20	0	2	0	0	0	91	1.6	3.5	−11.4	968	1,462	−27.2	1,377	1,907
Niger @ Niamey	6231	165	99	1	0	1	0.3	18	13	7	34	0	3	25	0	0	105	2.1	4.4	−10.5	985	1,523	−26.1	1,282	1,815
Niger @ Yantala	6074	380	98	2	0	0	0.7	0	9	0	24	5	12	50	0	0	43	0.8	3.9	−11.2	1,095	1,633	−21.6	1,315	1,944
Sokoto	6073	220	99	1	0	0	0.0	22	30	1	10	1	12	22	0	1	16	0.3	3.7	−12.9	1,145	1,635	−25.3	1,617	2,209
Ka	6076	55	94	3	3	0	1.2	6	14	6	47	0	8	18	0	1	179	3.7	4.6	−16.3	1,429	1,873	−34.4	1,678	2,143
Oli	6078	375	99	1	0	0	0.4	75	12	3	1	0	6	0	0	2	445	8.1	2.7	−18.2	1,727	2,155	−32.6	1,505	1,975
Kaduna	6080	750	100	0	0	0	0.4	81	12	1	0	0	4	0	0	0	135	2.5	9.1	−21.3	1,917	2,298	−35.8	1,723	2,175
Niger @ Adaha	6082	110	92	4	4	0	0.7	6	10	2	21	1	10	47	0	3	164	3.6	9.8	−19.8	1,854	2,257	−33.0	1,732	2,216
Niger @ Jamata	6232	49	83	12	5	1	1.7	16	7	2	24	0	12	38	0	0	1,318	34.3	24.6	−16.4	1,641	2,101	−27.3	1,293	1,808
Benue @ Ibi	6087	360	76	18	6	1	0.6	4	0	1	14	9	1	56	11	5	55	1.1	5.3	−12.7	1,058	1,532	−21.8	1,106	1,683
Shemanker	6086	400	62	24	15	0	1.1	40	1	2	11	3	0	35	0	8	132	2.8	9.0	−16.0	1,399	1,846	−20.5	1,010	1,588
Dep	6085	330	79	12	9	1	1.6	6	4	0	13	3	0	72	0	1	1,708	30.2	9.9	−10.2	906	1,430	−13.8	661	1,280
Mada	6084	150	56	30	13	0	2.3	9	0	0	13	1	0	76	0	0	624	10.2	4.4	−10.2	981	1,528	−21.1	974	1,526
Benue @ Shata	6090	340	79	17	4	0	0.4	1	6	0	28	7	4	47	6	1	85	1.7	6.8	−11.5	992	1,489	−19.9	1,012	1,605
Okwa	6083	710	90	6	1	3	1.5	4	21	0	5	4	38	25	0	1	110	2.7	5.8	−12.7	1,275	1,797	−19.9	1,007	1,599
Katsina Ala	6088	350	76	20	4	0	0.6	2	0	2	15	7	4	55	11	2	86	1.8	7.5	−13.9	1,114	1,565	−17.8	909	1,522
Benue @ Mozum	6233	46	56	25	19	0	2.8	5	0	2	16	2	1	69	1	3	1,359	36.0	32.4	−14.1	1,314	1,796	−20.5	972	1,536
Niger @ Itobe	6234	40	62	23	14	0	2.9	7	0	1	23	1	1	65	1	1	1,974	60.1	44.6	−17.1	1,670	2,117	−22.1	1,034	1,583
Niger @ Asaba	6092	345	89	6	4	0	0.3	2	2	1	20	6	4	63	1	1	37	0.7	6.0	−11.6	927	1,403	−22.3	1,244	1,842

Journal of Geophysical Research: Earth Surface
10.1029/2023JF007342

Table 1
Continued

River	Sample	GSZ (μm)	Q (%)	KF (%)	P (%)	L (%)	tHMC (%)	Zrn (%)	Tur (%)	TiOx (%)	Ep (%)	Grt (%)	SAKS (%)	Amp (%)	Px (%)	&tHM (%)	Zr (ppm)	Hf (ppm)	Nd (ppm)	ε_{Nd}	$T_{Nd,CHUR}$ (Ma)	$T_{Nd,DM}$ (Ma)	ε_{Hf}	$T_{Hf,CHUR}$ (Ma)	$T_{Hf,DM}$ (Ma)
Niger @ Patani	6103	350	95	4	2	0	0.3	13	6	2	26	3	9	38	0	2	174	3.4	7.0	−14.3	1,340	1,823	−23.6	1,164	1,716
Nun distributary	6104	180	89	7	3	1	0.5	10	5	1	29	1	6	43	0	3	359	5.9	6.5	−18.4	1,677	2,097	−25.5	1,211	1,739
Ogun	6100	140	79	11	10	0	1.9	3	4	0	7	1	10	71	0	1	727	15.5	10.2	−18.5	1,599	2,011	−28.9	1,332	1,829

Note. GSZ, grain size; Q, quartz; KF, K-feldspar; P, plagioclase; L, lithic fragments; tHMC, transparent heavy-mineral concentration; Zrn, zircon; Tur, tourmaline, TiOx, titanium oxides; Ep, epidote; Grt, garnet; SAKS, staurolite + andalusite + kyanite + sillimanite; Amp, amphibole; Px, pyroxene; &tHM, other transparent heavy minerals (mainly titanite, apatite, or olivine).

3.2. Detrital-Zircon Geochronology

From the heavy-mineral separation of 32 fluvial sands obtained by wet sieving (15–500 μm fraction) and of three bulk samples of eolian-dune sand, detrital zircons were concentrated with standard magnetic techniques, directly mounted in epoxy resin without any operator selection by hand picking, and identified by automated phase mapping (Vermeesch et al., 2017) with a Renishaw QONTOR™ Raman microscope. U-Pb zircon ages were determined at the London Geochronology Centre using an Agilent 7900 laser-ablation inductively coupled-plasma mass-spectrometry system, employing a NewWave NWR193 Excimer Laser operated at 10 Hz with a 25 μm spot size and ∼2.2 J/cm^2 fluence. No cathodoluminescence imaging was performed, and the laser spot was always placed blindly in the middle of zircon grains to treat all samples equally and avoid bias in intersample comparison ("blind-dating approach" discussed in Garzanti et al. (2018)). The mass spectrometer data were converted to isotopic ratios using *GLITTER 4.4.2* software (Griffin et al., 2008), employing Plešovice zircon (Sláma et al., 2008) as primary age standard and GJ-1 (Jackson et al., 2004) and 91500 (Wiedenbeck et al., 2004) as secondary age standards, obtaining average ages of 592.3 ± 0.9 (MSWD 2.4, n = 65) and 1,022.4 ± 3.1 (MSWD 0.8, n = 16), respectively. A NIST SRM612 glass was used as a compositional standard for U and Th concentrations. *GLITTER* files were post-processed using *IsoplotR 5.3* (Vermeesch, 2018). Concordia ages were calculated as the maximum likelihood intersection between the concordia curve and the error ellipse of $^{207}Pb/^{235}U$ and $^{206}Pb/^{238}U$ (Ludwig, 1998). The discordance cutoff was set at −5/+15 (Vermeesch, 2021). Zircon-age data are plotted as kernel density estimates (KDE) using the *provenance* package of Vermeesch et al. (2016). Statistical techniques used to illustrate our data set include multidimensional scaling (MDS), which produces a map of points in which the distance among samples is approximately proportional to the Kolmogorov-Smirnov dissimilarity of their compositional or chronological signatures; the goodness of fit is evaluated using the "stress" value of the configuration (0.2 = poor; 0.1 = fair; 0.05 = good; Vermeesch, 2013; Vermeesch & Garzanti, 2015). The complete geochronological data set of 6677 ages, 4299 of which are considered concordant (64% on average but ranging from only 28%–42% in Guinean headwaters to 78%–89% for Benue tributaries), is provided in Appendix S2 in Supporting Information S1.

Forward mixing calculations of zircon-age populations were made by both inverse Monte Carlo modeling with Kolmogorov-Smirnov and Kuiper test statistics (Sundell & Saylor, 2017) and Wasserstein statistics, a refined method more sensitive to the tails of the distribution (Lipp & Vermeesch, 2023). The best fit is obtained for the synthetic mixing proportion yielding the minimum Wasserstein distance to the spectrum of the outlet sample.

4. Detrital Zircon Ages

4.1. Upper Niger

In uppermost Niger sand, all ages are Archean (11% Neoarchean, 88% Mesoarchean, 1% Paleoarchean) (Figure 2). The youngest zircon age is 2.65 Ga (Liberian), the oldest is 3.39 Ga (Leonian), and the main peak is at 2.88 Ga, revealing provenance exclusively from the Man Shield. Only 42% of the obtained ages could be considered concordant. Archean ages prevail over Paleoproterozoic ages in Milo sand, whereas Paleoproterozoic ages prevail in Tinkisso sand and are overwhelming in Sankarani, Baoulè and Bagoé sands in the northeast (Table 2). Along the Upper Niger course, detrital zircons of Archean age are progressively diluted by Paleoproterozoic zircons supplied by tributaries draining the Birimian Baoulé-Bossi domain, which become predominant in the Inner Delta. Archean zircons display a major Liberian peak (2.88 Ga, n = 433) and a minor Leonian peak (3.20 Ga, n = 20); Paleoproterozoic zircons display a latest Rhyacian peak (2.07 Ga; n = 560). A few Pan-African ages appear as the rivers cut across the Neoproterozic strata of the Taoudeni Basin (Ediacaran peak at ∼570 Ma; n = 31).

4.2. Saharan Dunes and Sahelian Niger

In eolian dunes collected both south and north of the Niger River in Mali, zircon grains yielded 56%–62% Ediacaran to Cryogenian ages (peak at 615 ± 20 Ma; Table 2), 19%–20% Orosirian to Rhyacian ages, and only 3%–5% Archean ages. Dune sand in northernmost Burkina Faso yielded less Paleoproterozoic and a few more (4%) Early/Middle Jurassic ages (Figure 2).

In Sahelian Niger sand from Timbuktú to Niamey, detrital zircons display virtually the same U-Pb age spectrum as Saharan dune sands, with Neoproterozoic ages increasing downstream from 46% to 62% (peak at 603 ± 10 Ma; Table 2). Archean ages decrease from 6% to 2%, Orosirian to Rhyacian ages decrease from 26% to 20%, and Jurassic ages increase from 1% to 4%. The drastic change from dominantly mid-Paleoproterozoic

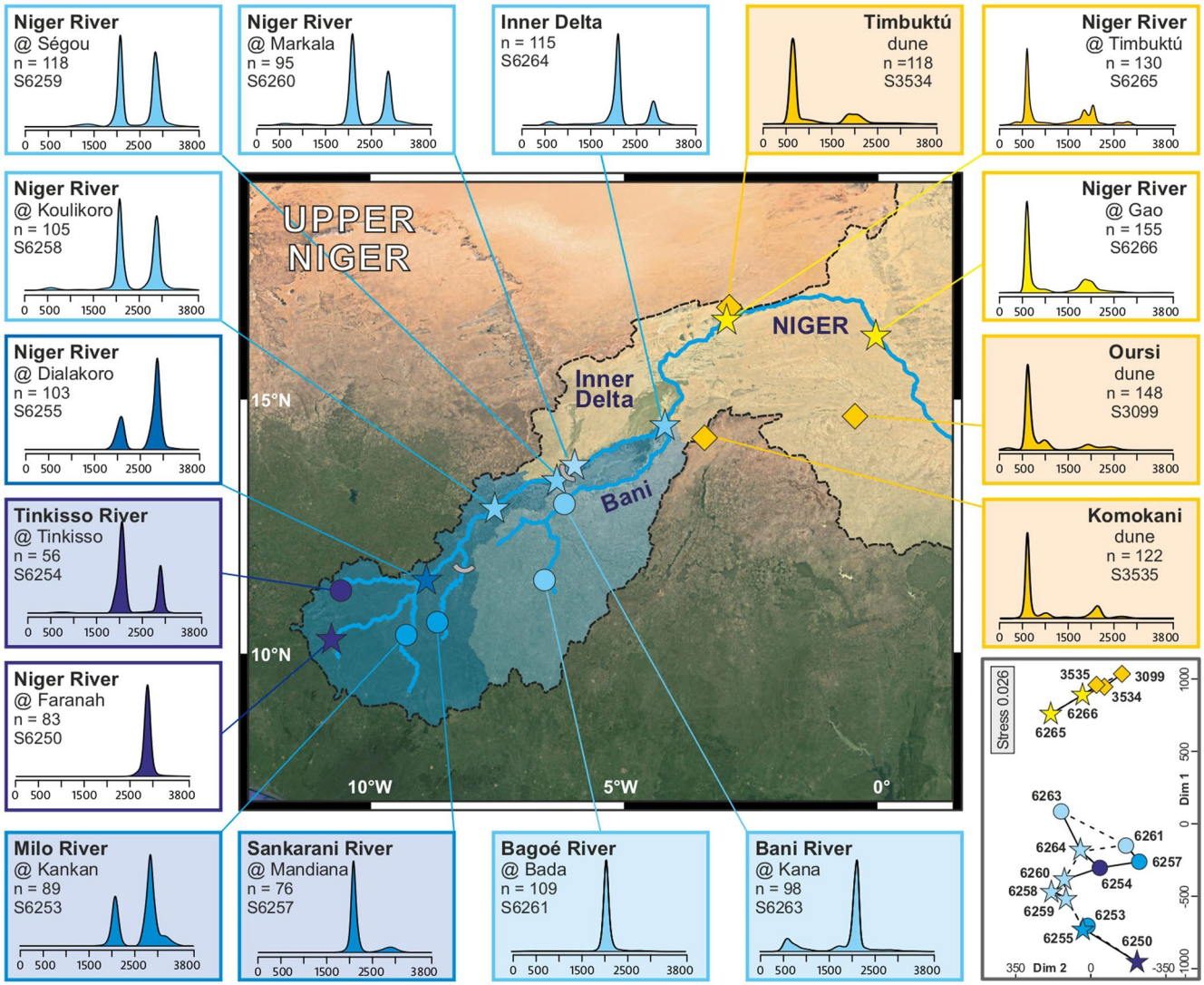

Figure 2. U-Pb age spectra of detrital zircons (white panels = Niger River; blue panels = tributaries; yellow panels = eolian dunes). Headwater Niger sand yielded exclusively Archean (>2.65 Ga) zircons derived from the Man Shield, Bagoé sand overwhelmingly ~2.1 Ga Birimian zircons. The MDS map in the bottom right panel highlights the disconnection of sediment transport across the Inner Delta; sediment load is reconstituted by recycling of Saharan dunes downstream (Figure 3).

and subordinately Mesoarchean ages in the Inner Delta to dominantly late Neoproterozoic ages downstream indicates that Upper Niger sediments are efficiently sequestered in the Inner Delta, and that Sahelian Niger sediments are virtually entirely reconstituted from erosion of eolian dunes across the edges of the Sahara sand sea (Figure 3).

4.3. Niger River in Nigeria

Neoproterozoic zircon grains are dominant in river sand throughout Nigeria, reflecting provenance from the Pan-African Trans-Saharan Belt (Figure 4). The sand of Middle Niger tributaries yielded a similar zircon-age spectrum. Sokoto sand contains 48% Ediacaran, 18% Cryogenian, 12% Paleoproterozoic, 6% Jurassic, and 3% Archean zircons. Ka sand yielded less Ediacaran-Cryogenian (49%) and more Statherian (16%) ages. The western Oli and eastern Kaduna tributaries, draining respectively the SW Nigeria and NW Nigeria basements, carry 57% Ediacaran and 29% Statherian to late Rhyacian zircons. Mixing of these various sources is reflected by the zircon grains carried by the Middle Niger, yielding 67% Neoproterozoic (mostly early/middle Ediacaran), 24% Paleoproterozoic (mainly late Rhyacian), and a few Jurassic (2%) and Archean (1%) ages. The SW Nigeria basement is also drained by the Ogun River, which is not part of the Niger catchment but debouches directly into the

Journal of Geophysical Research: Earth Surface
10.1029/2023JF007342

Table 2
U-Pb Age Peaks of Detrital Zircon Identified in Each Studied Sample

	Cretaceous			Jurassic			Permian-Carbon.			Pan-African			Tonian			Mesoproterozoic			Birimian			Liberian			Leonian		
River	Age	2σ	%	Age	2σ	%	Age	2σ	%	Age	2σ	%	Age	2σ	%	Age	2σ	%	Age	2σ	%	Age	2σ	%	Age	2σ	%
Niger @ Faranah	–	–	–	–	–	–	–	–	–	–	–	–	–	–	–	–	–	–	–	–	–	2875	20	100%	–	–	–
Tinkisso	–	–	–	–	–	–	–	–	–	–	–	–	753	8	2%	–	–	–	2044	21	68%	2877	50	30%	–	–	–
Milo	–	–	–	–	–	–	–	–	–	–	–	–	–	–	–	–	–	–	2081	28	70%	2901	36	30%	–	–	–
Niger @ Dialakoro	–	–	–	–	–	–	–	–	–	–	–	–	–	–	–	–	–	–	2081	26	29%	2875	18	67%	3206	163	4%
Sankarani	–	–	–	–	–	–	–	–	–	–	–	–	–	–	–	–	–	–	2093	15	86%	2870	70	14%	–	–	–
Niger @ Koulikoro	–	–	–	–	–	–	–	–	–	575	38	3%	–	–	–	–	–	–	2074	24	48%	2860	43	44%	3230	165	5%
Niger @ Ségou	–	–	–	–	–	–	–	–	–	–	–	–	–	–	–	1331	107	4%	2082	17	44%	2852	25	47%	3181	92	5%
Niger @ Markala	–	–	–	–	–	–	–	–	–	581	14	2%	–	–	–	1051	89	2%	2063	17	54%	2833	34	38%	3372	203	4%
Bagoé	–	–	–	–	–	–	–	–	–	561	33	2%	–	–	–	1040	168	3%	2076	14	93%	2786	40	2%	–	–	–
Bani	–	–	–	–	–	–	–	–	–	593	30	10%	849	73	9%	–	–	–	2074	26	75%	2761	207	6%	–	–	–
Inner Delta	–	–	–	–	–	–	–	–	–	594	26	4%	–	–	–	1547	154	6%	2052	16	64%	2856	38	26%	–	–	–
Niger @ Timbuktú	–	–	–	–	–	–	311	59	1%	592	14	49%	899	83	5%	1519	74	5%	1936	42	34%	2676	71	6%			
Niger @ Gao	–	–	–	–	–	–	–	–	–	605	9	56%	873	57	10%	–	–	–	1970	46	30%	2591	65	4%	–	–	–
Niger @ Niamey	–	–	–	189	29	5%	–	–	–	612	8	64%	–	–	–	–	–	–	2018	53	28%	2761	286	3%	–	–	–
Komokani dune	–	–	–	161	6	2%	–	–	–	596	9	49%	925	64	10%	1572	61	8%	1982	49	25%	2629	58	6%	–	–	–
Timbuktú dune	–	–	–	–	–	–	285	69	3%	635	10	47%	852	63	12%	1503	112	6%	1945	54	28%	–	–	–	3215	192	4%
Oursi dune	–	–	–	189	22	5%	–	–	–	613	9	58%	863	46	12%	–	–	–	1960	68	20%	2504	48	5%	–	–	–
Sokoto	–	–	–	175	9	6%	–	–	–	600	10	66%	941	54	12%	1639	65	2%	2044	69	11%	2538	45	3%	–	–	–
Ka	86	19	2%	–	–	–	–	–	–	589	12	48%	872	49	19%	1609	47	15%	1954	104	14%	2507	79	2%	–	–	–
Oli	–	–	–	175	2	1%	–	–	–	583	5	61%	838	44	1%	1574	48	16%	2011	47	21%	–	–	–	–	–	–
Kaduna	–	–	–	–	–	–	–	–	–	579	5	61%	–	–	–	1559	67	10%	2001	44	29%	–	–	–	–	–	–
Niger @ Adaha	–	–	–	165	8	2%	–	–	–	602	8	62%	849	65	8%	–	–	–	2087	58	28%	–	–	–	–	–	–
Niger @ Jamata	–	–	–	162	24	2%	–	–	–	606	9	58%	896	47	16%	–	–	–	2035	64	24%	–	–	–	–	–	–
Benue @ Ibi	–	–	–	171	5	1%	–	–	–	583	8	89%	839	64	4%	–	–	–	1941	85	6%	–	–	–	–	–	–
Shemanker	–	–	–	151	7	1%	–	–	–	580	5	99%	–	–	–	–	–	–	–	–	–	–	–	–	–	–	–
Dep	–	–	–	146	18	2%	–	–	–	626	28	18%	912	12	79%	1670	14	1%	–	–	–	–	–	–	–	–	–
Mada	–	–	–	–	–	–	–	–	–	587	5	99%	–	–	–	–	–	–	2035	45	1%	–	–	–	–	–	–
Okwa	–	–	–	147	6	4%	–	–	–	585	11	83%	844	64	13%	–	–	–	–	–	–	–	–	–	–	–	–
Katsina Ala	85	58	2%	–	–	–	–	–	–	602	8	77%	838	80	5%	1541	112	4%	2011	129	12%	–	–	–	–	–	–
Benue @ Mozum	–	–	–	–	–	–	–	–	–	604	8	83%	877	65	8%	–	–	–	1950	98	9%	–	–	–	–	–	–
Niger @ Itobe	–	–	–	–	–	–	–	–	–	608	7	89%	866	48	8%	–	–	–	1995	120	3%	–	–	–	–	–	–
Niger @ Asaba	72	8	1%	176	26	2%	–	–	–	602	8	77%	859	54	7%	–	–	–	1989	84	10%	2555	71	2%	3331	22	1%
Niger @ Patani	–	–	–	176	16	4%	–	–	–	607	8	68%	926	53	13%	–	–	–	1950	78	12%	2786	245	3%	–	–	–
Nun distributary	69	2	1%	179	13	2%	–	–	–	590	9	82%	877	53	–	–	–	–	1885	57	12%	2499	44	3%	–	–	–
Ogun	–	–	–	–	–	–	–	–	–	604	9	45%	811	49	12%	–	–	–	2124	44	40%	2510	62	3%	–	–	–

Note. Central age, standard deviation, and proportions are calculated with *IsoplotR 5.3* (Vermeesch, 2018), implementing the discrete mixture modeling algorithms of Galbraith and Laslett (1993).

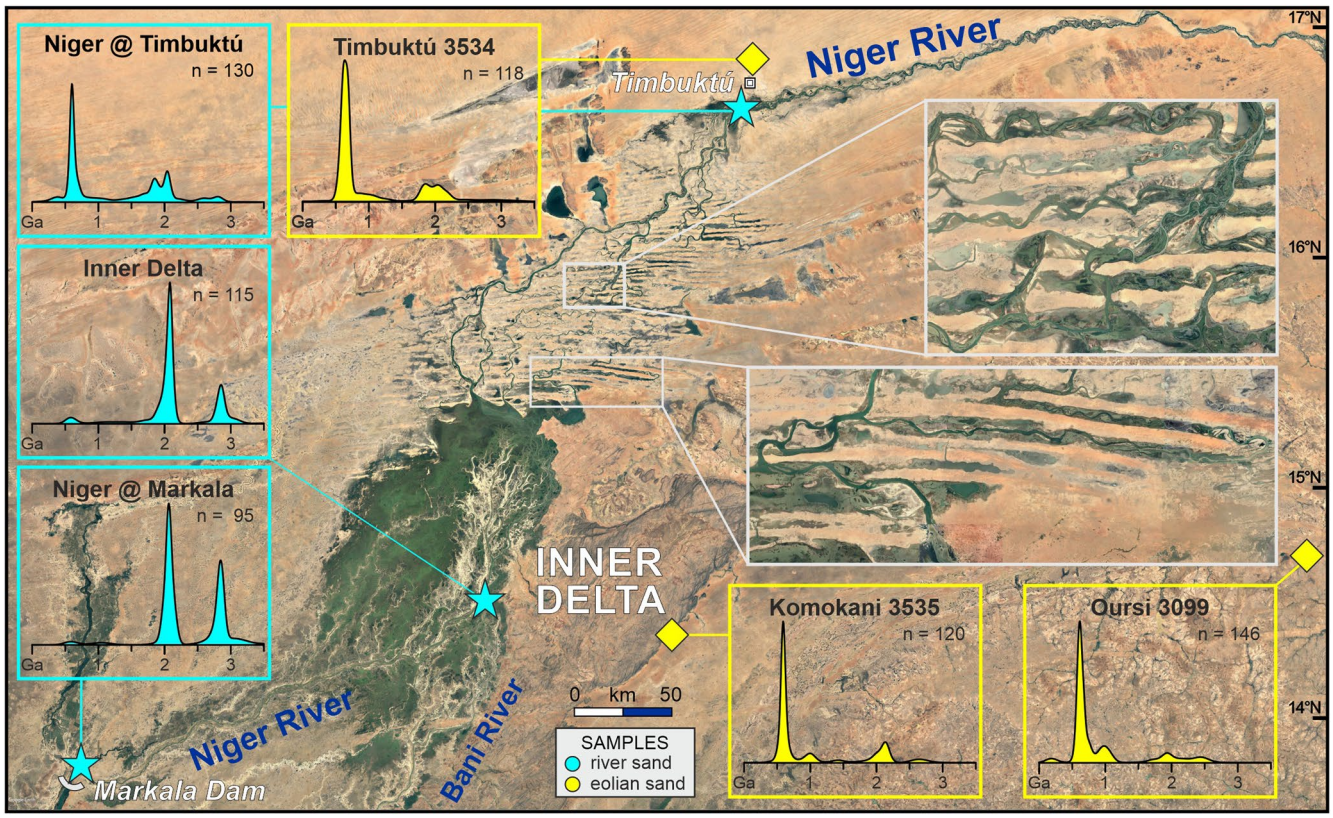

Figure 3. Fluvial-eolian interaction at the southern edge of the Sahara Desert. The flow of the Niger and Bani rivers is hampered at the entrance of the dune field, and sediment derived from Mesoarchean to Paleoproterozoic rocks exposed in the headwaters is dumped in the Inner Delta marshes. Downstream, the reduced discharge is partitioned in many streamlets that meander around E/W-trending dunes, while bedload is reconstituted by recycling of eolian sand with a late Neoproterozoic zircon-age signature.

Gulf of Guinea. Ogun sand contains a larger proportion of Paleoproterozoic zircons (41%, mainly Rhyacian with peak at ~2.1 Ga) associated with late Neoproterozoic grains (33% Ediacaran, 20% Cryogenian).

In the Benue catchment, zircon ages are overwhelmingly Neoproterozoic, mostly Ediacaran (up to 83%–85% for Shemanker and Mada sands, and 60%–69% for Katsina-Ala, Upper Benue and Okwa sands) and subordinately Cryogenian (9%–27%) (Figure 4). Dep sand yielded a different age spectrum with 78% Tonian zircons (peak at ~950 Ma). A few Jurassic zircons are carried by northern tributaries sourced in the Jos Plateau, and one Early Cretaceous and one Eocene grain were dated in Katsina-Ala sand. Archean grains are invariably <1%; Paleoproterozoic zircons occur in Benue and Katsina-Ala sands (8% and 10%, respectively) and are rare but increase progressively westward in northern tributaries (from 0.6% in Shemanker sand to 1.8% in Okwa sand).

Sand in the Lower Niger and Niger Delta distributaries yielded mostly Ediacaran (56% ± 6%) and subordinately Cryogenian (20% ± 3%) zircons, together with 1% Archean, 9% Paleoproterozoic, and 2% Jurassic zircons; two grains yielded ages as young as 6 and 1 Ma.

4.4. Size Distributions of Zircon Grains

The studied detrital-zircon populations are mostly in the very fine sand range, well sorted, and roughly symmetrical (sample mean 3.36 ± 0.46 ϕ, sorting 0.49 ± 0.09 $\sigma\phi$, skewness 0.02 ± 0.09). Zircon grains are finer in Upper Niger samples (3.58 ± 0.38 ϕ, 0.45 ± 0.07 $\sigma\phi$) and virtually identical in Sahelian Niger (3.37 ± 0.37 ϕ, 0.40 ± 0.09 $\sigma\phi$) and Saharan dune samples (3.33 ϕ, 0.40 $\sigma\phi$). In the Benue catchment, zircon grains tend to be coarser (2.97 ± 0.44 ϕ, 0.56 ± 0.11 $\sigma\phi$) and even coarser than predicted by the settling-equivalence principle in a few samples (e.g., 6085 and 6090 in Figure 5), which may indicate inheritance from relatively large zircon crystals in granitoid source rocks.

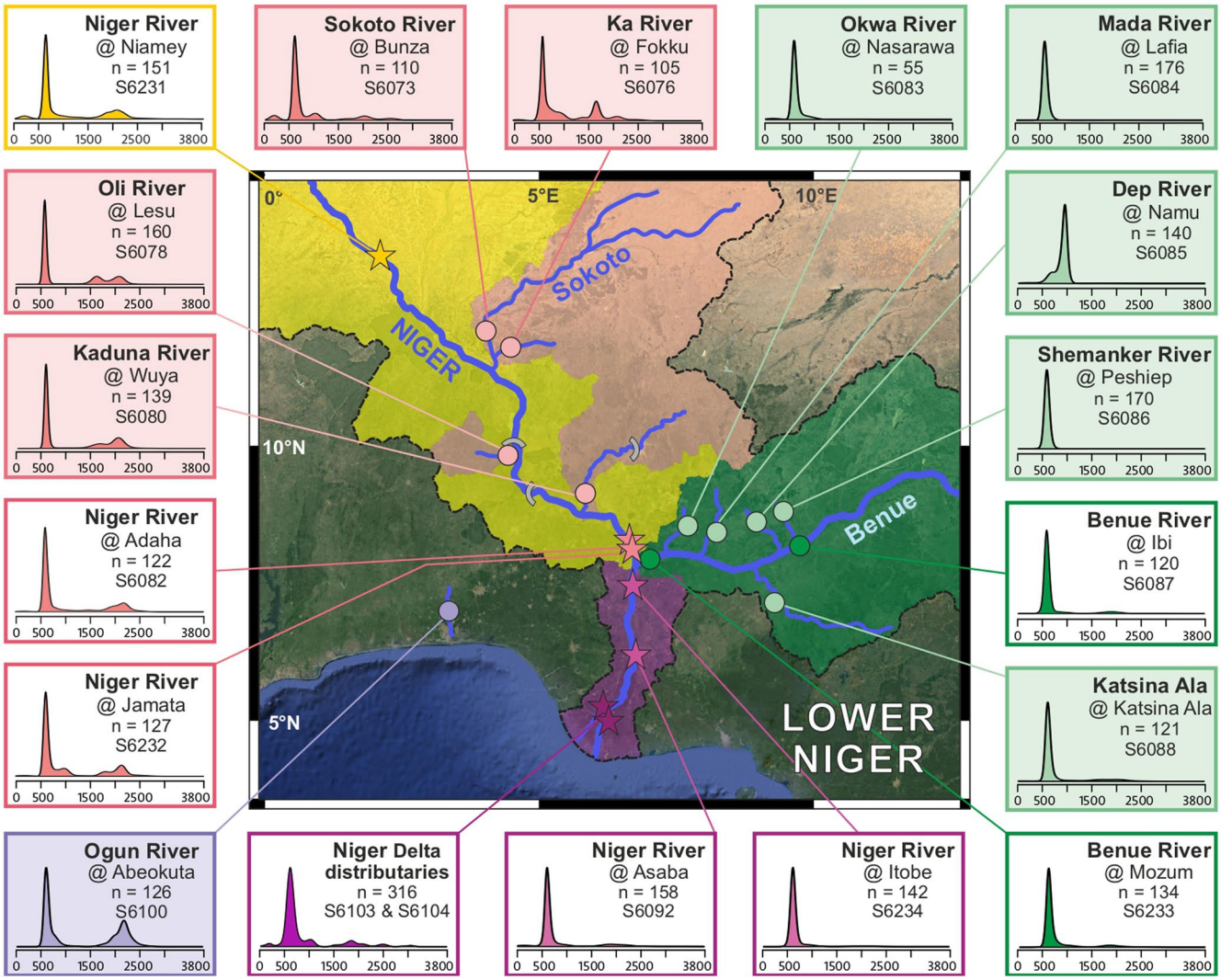

Figure 4. U-Pb age spectra of detrital zircons (white panels = Niger and Benue rivers; pink panels = Middle Niger tributaries; green panels = Benue tributaries; lilac panel = coastal river). Ediacaran zircons are dominant throughout the Benue catchment (but for the Dep River carrying mostly Tonian grains), whereas Paleoproterozoic zircons commonly occur in Middle Niger tributaries and especially in the Ogun River sourced in the SW Nigeria basement.

4.5. Age Discordance and Degree of Metamictization

The percentage of concordant ages decreases regularly in samples with older zircon grains, which reflects a higher degree of metamictization consequent to the progressive accumulation of radiation dose since crystallization (Resentini et al., 2020). A lower degree of crystallinity owing to metamictization favors lead diffusion and weathering. A great number of very old zircon grains in Guinea show a linear trend of Pb diffusion/common lead mixing, and their highly metamict state is confirmed by the correlation with elements (e.g., lanthanum) not originally present in the zircon lattice but detected in significant amounts in weathered radiation-damaged crystals (Andersen & Elburg, 2022; Andersen et al., 2019).

Only 28%–42% of the obtained ages are concordant in Upper Niger headwater sands draining the Archean Man Shield in Guinea (samples 6250, 6253, 6254, 6257). This percentage reaches 48%–60% in sand mostly generated in the Paleoproterozoic Baoulé-Mossi (Birimian) domain in Mali, and systematically higher values downstream of the Inner Delta (61%–75% in Saharan dunes, 76%–78% in the Sahelian Niger; 75% ± 10% in Nigeria), where most zircons yielded Neoproterozoic ages. The percentage of concordant ages increases with grain size in Middle Niger (from 55% to 64% in very fine sand to 70%–82% in coarser sand), Benue (from 70% in very fine sand to 78%–89% in coarser sand), and Lower Niger samples (from 72% in very fine sand to 78%–81% in coarser sand). Such a distinct behavior is not an artifact caused by sample preparation or by mixing age domains during analysis,

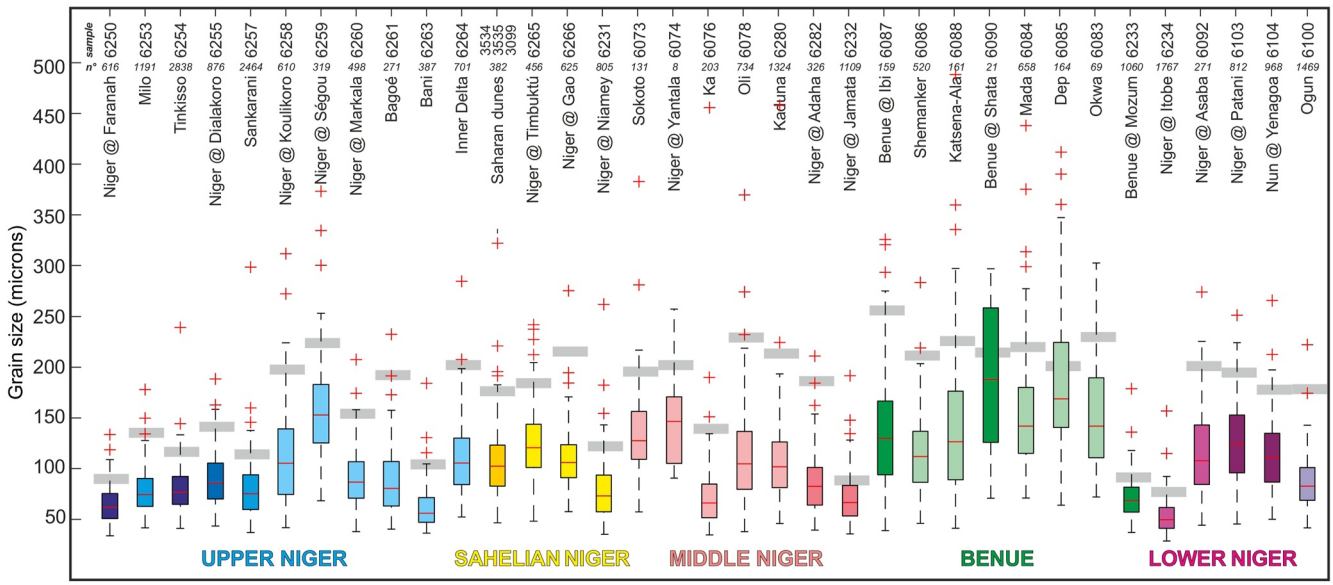

Figure 5. The size distribution of detrital zircons in the Niger catchment ($n°$ = number of analyzed zircon grains; boxes extend from the 25th to the 75th percentile, median is indicated by central red mark and outliers by red crosses; gray bars show average size of bulk 15–500 μm fraction). In a very fine to fine quartz-rich sand deposited by a tractive current, zircon grains are expected to be ~0.6 ϕ finer than bulk-sample grain size (Garzanti et al., 2008).

but it is a genuine characteristic of moderately to strongly metamict Upper Niger zircon populations, in contrast with the moderately high crystallinity of zircon grains entrained by the Sahelian Niger, Middle Niger, Benue River, and Lower Niger (Figure 6).

5. Geochemical Data

5.1. Zircon and Zr Concentrations

Zircon concentration can be independently estimated based on mineralogical and geochemical data in the diverse reaches of the Niger drainage basin (Table 1). In the Upper Niger catchment, integrated petrographic and heavy-mineral data indicate that zircon represents 0.14% ± 0.09% of the sand shed from largely Archean rocks in Guinea, about twice as much as for sand shed from the Paleoproterozoic Baoulé-Mossi (Birimian) rocks exposed in the Bani catchment (0.06% ± 0.03%). Because of extensive recycling of zircon-poorer Proterozoic sandstones of the Siguiri and Taoudeni basins, zircon concentration in Upper Niger sand decreases downstream in Mali, attaining a median value of 0.05%. This is confirmed by geochemical data: Zr concentrations are invariably higher in Guinea tributaries (Zr 346–1,428 ppm, average 749 ppm) than in the Bani catchment (Zr 98–313 ppm) and decrease steadily from Guinea headwaters (Zr 746 ± 77 ppm) to Mali (Zr mostly <100 ppm).

Zircon and Zr concentrations decrease further in Sahelian Niger sand, where they are as low as in Saharan dunes (zircon 0.03% ± 0.01% vs. 0.03% ± 0.03%, Zr 87 ± 12 vs. 72 ± 17 ppm), and increase again progressively in Nigeria, indicating that zircon fertility of granitoid basement rocks is higher than for sedimentary covers by up to an order of magnitude. Zircon and Zr concentrations are 0.06% ± 0.06% and 174 ± 138 ppm for Middle Niger mainstem and tributaries, and highly variable in the sand of Benue mainstem and tributaries (0.07% ± 0.06% and mainly 88 ± 30 ppm but locally up to 624 and 1,708 ppm in Mada and Dep sands, respectively). In the Lower Niger sand, zircon and Zr concentrations vary strongly from 0.008% to 37 ppm to 0.12% and 630 ppm.

5.2. HREE Patterns

Because zircon contains significant amounts of the heaviest REEs, HREE patterns in Niger sand are largely controlled by zircon content. The Gd_N/Yb_N ratio correlates negatively with Zr concentration ($r = -0.53$, sign. lev. <0.1%) and Zr and Hf concentrations correlate best with the concentration of Yb and Lu ($r = 0.89$–0.92). HREE fractionation varies notably (Gd_N/Yb_N from 0.4 in Dep sand to 3.3 in Kaduna sand), and it is lower in Upper Niger (1.2 ± 0.5), Saharan-dune (Gd_N/Yb_N 1.3 ± 0.1), and Middle Niger sands (Gd_N/Yb_N 1.5 ± 0.1) than in Benue (Gd_N/Yb_N 2.0 ± 0.7) and Lower Niger sands (Gd_N/Yb_N 1.9 ± 0.6).

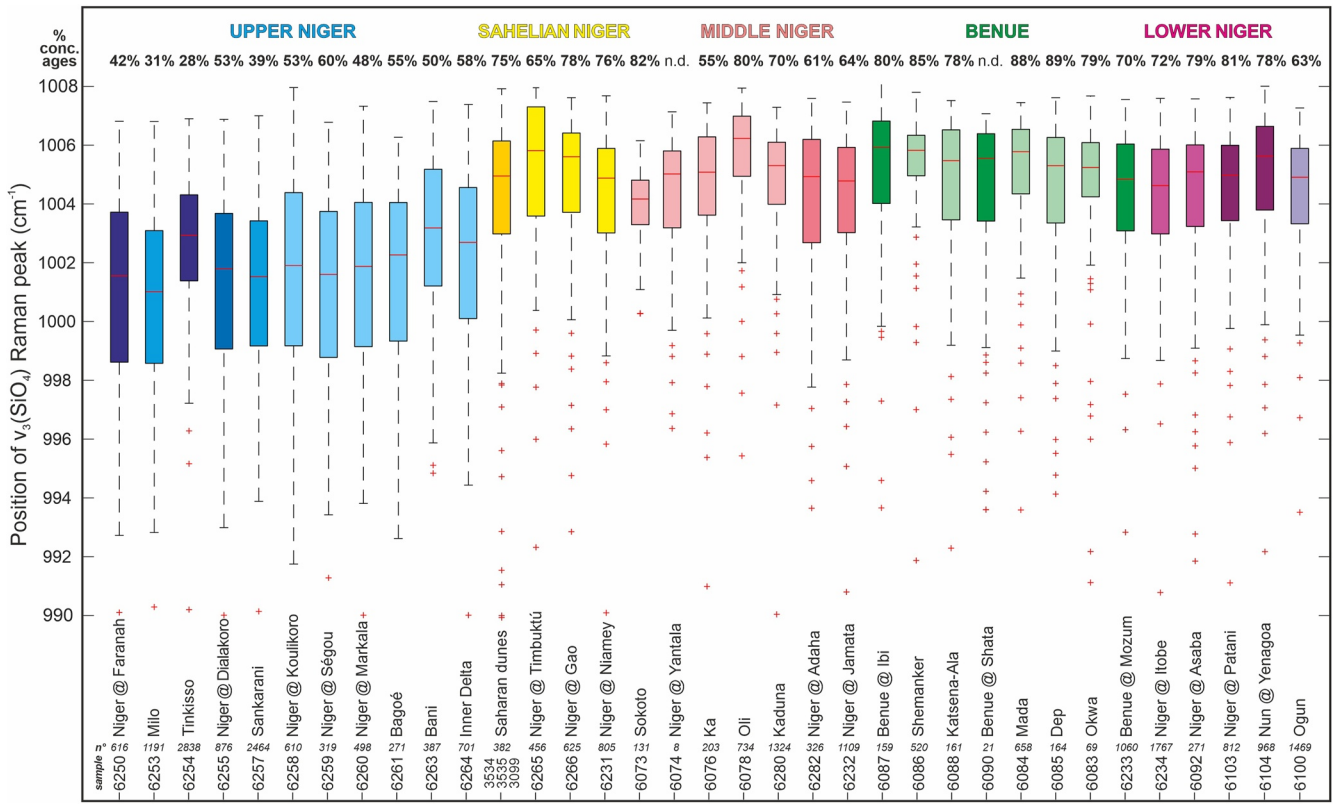

Figure 6. The degree of zircon metamictization revealed by $v_3(SiO_4)$ Raman peak position (Nasdala et al., 1995; $n°$ = number of analyzed zircon grains; boxes extend from the 25th to the 75th percentile, median is indicated by central red mark and outliers by red crosses). Archean to Paleoproterozoic zircons in Upper Niger sand yield a higher percentage of discordant ages (53% ± 11% vs. 25% ± 9% in other sands) and display a higher degree of metamictization [i.e., $v_3(SiO_4)$ peak shifted to lower wavenumbers].

By considering that the Lu/Hf ratio is much lower in zircon (~0.002; Kinny & Maas, 2003) than in the upper continental crust (~0.055; Taylor & Mclennan, 1995), the average Lu/Hf value of 0.026 (although with wide variations among samples from 0.006 to 0.072) implies that zircon accounts for at least half of the Lu budget overall.

5.3. Zr/Hf Ratio

The Zr/Hf ratio in sediments is strongly controlled by grain size, being typically close to the chondritic value of ~37 in mud and to the average zircon value of ~47 in sand (Bea et al., 2006; Garzanti, Bayon, Vermeesch, et al., 2022). In magmatic rocks, Zr/Hf decreases regularly with progressive differentiation (Wang et al., 2010), allowing the distinction of common granites (Zr/Hf > 55) from moderately evolved (25 < Zr/Hf < 55) and highly evolved granites (Zr/Hf < 25; Breiter et al., 2014; Wu et al., 2017).

Within our sample set, the Zr/Hf ratio is much lower in the Upper Niger catchment (42 ± 3) than in Saharan dunes (60 ± 2) and ranges widely in Nigeria (between 46 and 55 in the Middle Niger catchment, and between 41 and 61 in the Benue catchment). Downstream of the Benue confluence, Zr/Hf increases from 51 to 52 in medium sand of the Lower Niger to 61–69 in fine sand of deltaic distributaries, which is significantly higher than in Ogun sand (47).

The seven highest Zr/Hf ratios were obtained for pure quartzose Saharan-dune sands (58–62; zircon accounting for 0.01%–0.06% of total sample), quartz-rich feldspatho-quartzose to pure quartzose delta-distributary sands (61–69; zircon accounting for 0.05%–0.06% of total sample), and feldspatho-quartzose Dep and K-feldspar-rich feldspatho-quartzose Mada sand (57–61; zircon accounting for 0.08%–0.25% of total sample), indicating common granite protosources. Ratios close to the expected value for mud (Zr/Hf 36 ± 3) were obtained from the three very coarse silt samples collected upstream and downstream of the Niger/Benue confluence. In sand, ratios

significantly lower than expected were obtained across the Upper Niger catchment (Zr/Hf 42 ± 3) but in Nigeria only for coarse quartzose Okwa sand (Zr/Hf 41), signaling the only local occurrence of evolved granites in the Trans-Saharan Belt.

5.4. Zirconium Budget

In zircon crystals grown in a variety of igneous and metamorphic rocks, the concentration of Zr is on average ∼49% (close to the stoichiometric value of 49.76%), with the Zr/Hf ratio ranging widely between 20 and 70 (Bea et al., 2006). Most common minerals have Zr concentrations well below that of the average upper continental crust (i.e., ∼200 ppm; Rudnick & Gao, 2003) and among them only titanite, some amphiboles, or allanite may occasionally reach a Zr concentration well above 1,000 ppm (Deer et al., 1997). Such minerals, however, are not sufficiently abundant to have a significant impact on Zr and Hf budgets (Garzanti & Andò, 2007). Among common silicates, only quartz may be abundant enough, despite its low Zr and Hf concentration (indicatively 35 and ∼1 ppm, respectively; Garzanti et al., 2010).

Based on Zr and Hf concentration in different detrital minerals (data after Bea et al. (2006)), zircon is estimated to account on average for 87% of the Zr budget, and feldspars for less than 3% for Sahelian and Middle Niger sands but up to ∼5% for uppermost Niger and Benue sands. Quartz is estimated to account for 11% of the Zr budget on average, but even for a half or more in a few pure quartzose samples. No correlation was observed between the Zr/Hf ratio and the estimated relative contributions of zircon and quartz.

5.5. Neodymium and Hafnium Isotopes

Isotopic ratios represent very useful additional tools to unravel provenance and constrain sediment budgets. Specifically, hafnium isotopes in bulk sand represent a valuable complement to detrital-zircon ages, considering that no less than 65%–70% of upper crustal hafnium is estimated to be hosted in zircon (Van de Flierdt et al., 2007).

Extremely negative epsilon values characterize uppermost Niger sand generated entirely from the Archean Kénéma-Man domain in Guinea (ε_{Nd} −41 and ε_{Hf} −67, corresponding to earliest Paleoarchean and latest Eoarchean $T_{Nd,CHUR}$ and $T_{Nd,DM}$ model ages, and to mid-Mesoarchean and latest Paleoarchean $T_{Hf,CHUR}$ and $T_{Hf,DM}$ model ages; Table 1). Because of mixing with sediment derived from Paleoproterozoic and finally Neoproterozoic rocks, epsilon values become progressively less negative downstream the Upper Niger (ε_{Nd} −23 and ε_{Hf} −43 in Inner Delta sand, corresponding to Orosirian and late Siderian $T_{Nd,CHUR}$ and $T_{Nd,DM}$ model ages and to Rhyacian and latest Neoarchean $T_{Hf,CHUR}$ and $T_{Hf,DM}$ model ages; Table 1). Epsilon values are less negative in the sand of the Bani tributary draining the Paleoproterozoic Birimian domain in northern Ivory Coast and southernmost Mali (ε_{Nd} −19 and ε_{Hf} −38, corresponding to model ages ranging from early Calymmian to Rhyacian; Table 1).

Epsilon values abruptly become less negative in Sahelian Niger sand (ε_{Nd} and ε_{Hf} from −23 and −43 in the Inner Delta to −10 and −26 in Niger, corresponding to model ages decreasing from Orosirian/late Neoarchean to Tonian/Orosirian). Such a decrease reflects extensive recycling of Saharan dunes (ε_{Nd} −12 ± 1 and ε_{Hf} −32 ± 5, corresponding to Tonian/Stenian $T_{Nd,CHUR}$ and Calymmian $T_{Nd,DM}$ model ages and to Ectasian/Orosirian $T_{Hf,CHUR}$ and Paleoproterozoic $T_{Hf,DM}$ model ages; Table 1) and ultimate provenance from the Neoproterozoic Trans-Saharan Belt. A significant change downstream of the Inner Delta is observed also for ε_{Nd} values in clay (own data).

Epsilon values become progressively more negative downstream of the Middle Niger, both in the mainstem (ε_{Nd} and ε_{Hf} down to −20 and −33, corresponding to Paleoproterozoic model ages) and in tributaries (from ε_{Nd} −13 and ε_{Hf} −25 in Sokoto sand to ε_{Nd} −21 and ε_{Hf} −36 in Kaduna sand), reflecting increasing detritus from the Nigeria basement complex.

Epsilon values are less negative and more homogeneous across the Benue catchment (ε_{Nd} −13 ± 2 and ε_{Hf} −19 ± 3, corresponding to Tonian/Ectasian $T_{Nd,CHUR}$, mostly Calymmian/Statherian $T_{Nd,DM}$, mostly Tonian/Stenian $T_{Hf,CHUR}$, and mostly Ectasian/Calymmian $T_{Hf,DM}$ model ages) than in the Lower Niger (where they tend to become more negative downstream from ε_{Nd} −14 ± 4 and ε_{Hf} −16 ± 3 to ε_{Nd} −22.2 ± 0.1 and ε_{Hf} −25 ± 1).

Table 3
Zircon Provenance Budgets Based on the Iterative Method of Garzanti et al. (2019) With Wasserstein (Wa) Statistics (Lipp & Vermeesch, 2023), and on Inverse Monte Carlo Modeling With Kuiper (Ku) and Kolmogorov-Smirnov (KS) Test Statistics (Sundell & Saylor, 2017)

River	Wa (%)	Ku (%)	KS (%)	Fluvial reach
Upper Niger	49	30	30	*Inland Delta*
Bani	51	70	70	
Inland Delta	12	12	6	*Sahelian Niger*
Sahara dunes	88	88	94	
Sahelian Niger	57	43	65	
Sokoto	40	42	14	*Middle Niger*
Ka	1	8	7	
Oli	1	4	7	
Kaduna	1	4	7	
Middle Niger	12	11	10	*Lower Niger*
Benue	88	89	90	

6. The Zircon Budget

In this section, U-Pb age distributions are considered as fingerprints of different source-rock domains and used to quantitatively assess the provenance of zircon grains in different parts of the Niger catchment. It must be underscored that the results of such an exercise cannot be directly translated into a sediment budget for a variety of reasons (Vezzoli et al., 2016). First, these estimates would need to be corrected for zircon concentrations, which may vary strongly among different potential sediment sources and can hardly be assessed with the required precision (Malusà et al., 2016). Second, sediment composition cannot be safely assumed as grain-size invariant, and results based on bedload sand may not be applicable to the mud fraction carried in suspension, which represents the largest part of the sediment flux by far. Third, inhomogeneities in sediment mixing in the fluvial system are caused by different grain-size distributions and/or seasonal variations in tributary versus mainstem sediment fluxes, local reworking of loose deposits (e.g., terraces, alluvial fans at confluences, eolian dunes) and anthropogenic effects (e.g., dam construction). Consequently, the estimated relative contributions suffer from the intrinsic variability of complex natural phenomena and are non-unique and uncertain (Garzanti et al., 2012; Resentini et al., 2017), even more so when they are based on a rare mineral such as zircon that occurs only in a limited range of source rocks (chiefly granitoids/metagranitoids and sandstones/metasandstones) and represents far less than a ten thousandth of the sediment load. Moreover, the unmixing of detrital-geochronology data can be done in various ways and under a range of assumptions, which, on the other hand, allows us to verify the robustness of the outcomes and obtain an empirical estimate of the associated uncertainty (Table 3).

6.1. Zircon Provenance Budget

Zircon mixing proportions in various reaches of the Niger course were estimated by combining different approaches (Table 3). Zircon grains in our Inner Delta sample are calculated to be derived slightly more from the Bani River (51%–70%) than from the Upper Niger (30%–49%), and most zircon grains in the Sahelian Niger (88%–94%) appear to be recycled from Saharan dunes, with only a minority (≤12%) derived from upstream of the Inner Delta. This reflects transport disconnection between the Upper Niger and the Sahelian Niger because of sediment dumping in the Inner Delta (Figure 7).

Zircon grains in Middle Niger sand are calculated to be supplied in subequal proportions by the Sahelian Niger (43%–65%) and by tributaries (14%–42% from Sokoto, 7%–8% from Ka, and 8%–14% from Oli and Kaduna combined). Finally, most zircon grains in the Lower Niger and Niger Delta appear to be supplied in much greater proportion by the Benue River (≥88%) than by the Middle Niger (≤12%), which carries many more Paleoproterozoic grains (24% ± 1%) than Benue (7% ± 2%) and Lower Niger (9% ± 4%) sands (Figure 8).

6.2. Inferences on Sand Provenance

The zircon provenance budget (Table 3), combined with zircon and zirconium concentrations appraised from integrated petrographic, heavy-mineral, and geochemical data in different parts of the Niger drainage basin (Table 1), allows us to tentatively draw semi-quantitative indications on bulk-sand provenance. If our assumptions are correct, then a zircon concentration of 0.05%–0.06% in both Upper Niger and Bani sands implies that our Inner Delta sample was fed in subequal proportions by the Upper Niger and its Bani tributary. Three explanations are viable: (a) sand production is more efficient in the Bani catchment than in the Upper Niger catchment, which is however in contrast with notably greater water discharge and sediment yields for the Upper Niger (7–8 t $km^{-2}a^{-1}$) than for the Bani River (3 t km^{-2} a^{-1}; Olivry, 1995, 1998); (b) larger dams on the Upper Niger (e.g., Selingué Dam completed in 1982 on the Sankarani tributary, Markala Dam completed in 1947 on the mainstem; Ferry et al., 2012) may have sequestered a significant part of Upper Niger sand in the reservoir; (c) our sample is not representative of the average composition of Inner Delta sand.

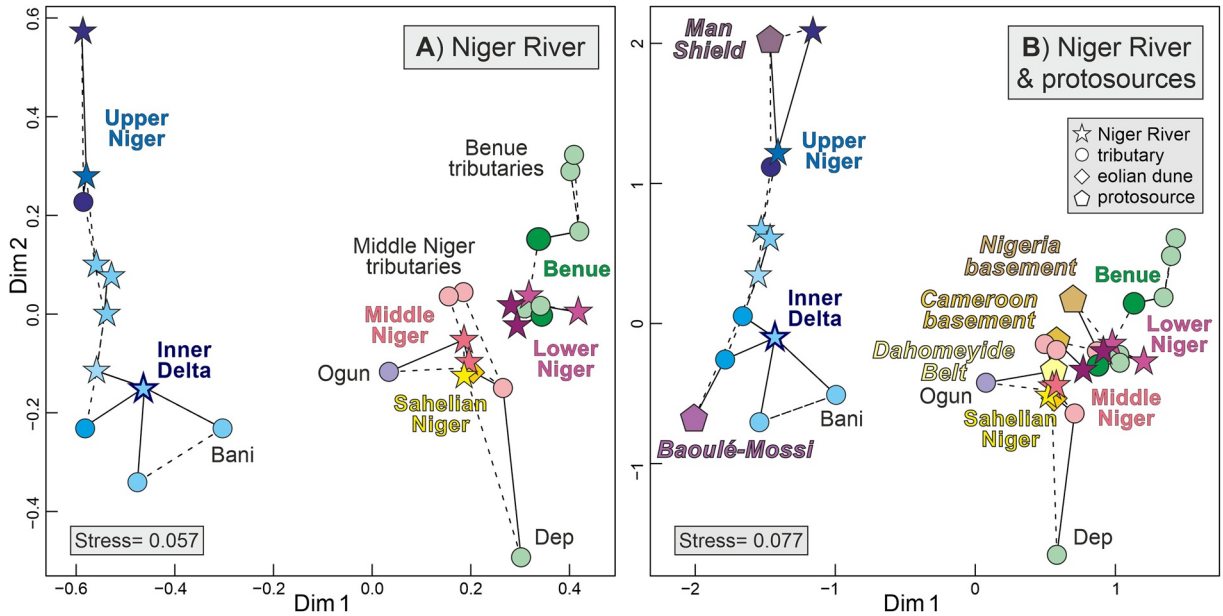

Figure 7. Multidimensional scaling maps based on U-Pb zircon-age spectra highlight the segmentation of the Niger sediment-transport system (closest and second-closest neighbors are linked by solid and dashed lines, respectively). (a) The Upper Niger is disconnected from the Sahelian Niger downstream of the Inner Delta, and zircons in the Lower Niger are overwhelmingly supplied by the Benue River. (b) Zircons in the Upper Niger are supplied by Archean (Man Shield) and Paleoproterozoic (Baoulé-Mossi) protosources (data from Table 4), whereas zircon grains are mostly derived from the Neoproterozoic (Trans-Saharan Belt) protosource downstream of the Inner Delta.

A zircon concentration of 0.06%–0.07% is estimated for both Middle Niger mainstem and tributaries and Benue mainstem and tributaries, indicating that most (~90%) Lower Niger sand is supplied by the Benue River rather than by the Middle Niger. The predominance of Benue supply is confirmed by forward mixing calculations based on Nd isotope data (Table 1), suggesting that 89% ± 9% of the REEs in Lower Niger sand are derived from the Benue River and 11% ± 9% from the Middle Niger. Hf isotope data confirm a predominant, although less overwhelming, prevalence of Benue contribution (77% ± 5%). More efficient sediment production in the Benue catchment than in the Middle Niger catchment is indicated unless a substantial amount of Middle Niger sediment is sequestered in large reservoirs upstream (e.g., Kainji and Shiroro lakes; Daramola et al., 2022; Ogunkoya, 2023).

6.3. Segmented Sediment-Transport Systems: Causes and Consequences

In most modern river systems, a continuous sediment flux from the headwaters to the mouth has been prevented by extensive human activities, including the construction of countless small, medium, and large dams since the dawn of civilization. The second half of the last century has seen an acceleration of dam construction worldwide for flood regulation, water supply and hydropower, including huge dams capable of sequestering virtually all sediment load in the reservoir behind. As a result, sediment delivery to the ocean from big rivers such as the Nile or the Indus has been drastically reduced to virtually zero (Stanley & Warne, 1998; Syvitski et al., 2013). This is partly true also for the Niger River, where dams built both on the Upper Niger and Middle Niger have reduced the sediment flux downstream by an undetermined amount.

Segmentation of fluvial sediment transport, however, is by no means an exclusively Anthropocene phenomenon and it has natural causes as well. Natural barriers to sediment-transport continuity include large lakes found in both orogenic and anorogenic settings. For instance, detritus generated in the headwaters of rivers sourced from the entire East African rift, from the Shire River in Malawi to the White Nile in Uganda, is trapped in large natural lakes. Similarly, detritus generated in the headwaters of Alpine rivers is blocked in lakes shaped by glaciers along both the northern and southern flanks of the European Alps (Hinderer, 2001). Another effective barrier to sediment transport is represented by vast marshlands formed in subsiding areas of cratonic interiors, such as the Sudd on the White Nile in South Sudan (Garzanti et al., 2015) and the Pantanal on the Paraguay River in South America (Assine et al., 2015), or by inland deltas such as those formed by the Okavango River in Botswana

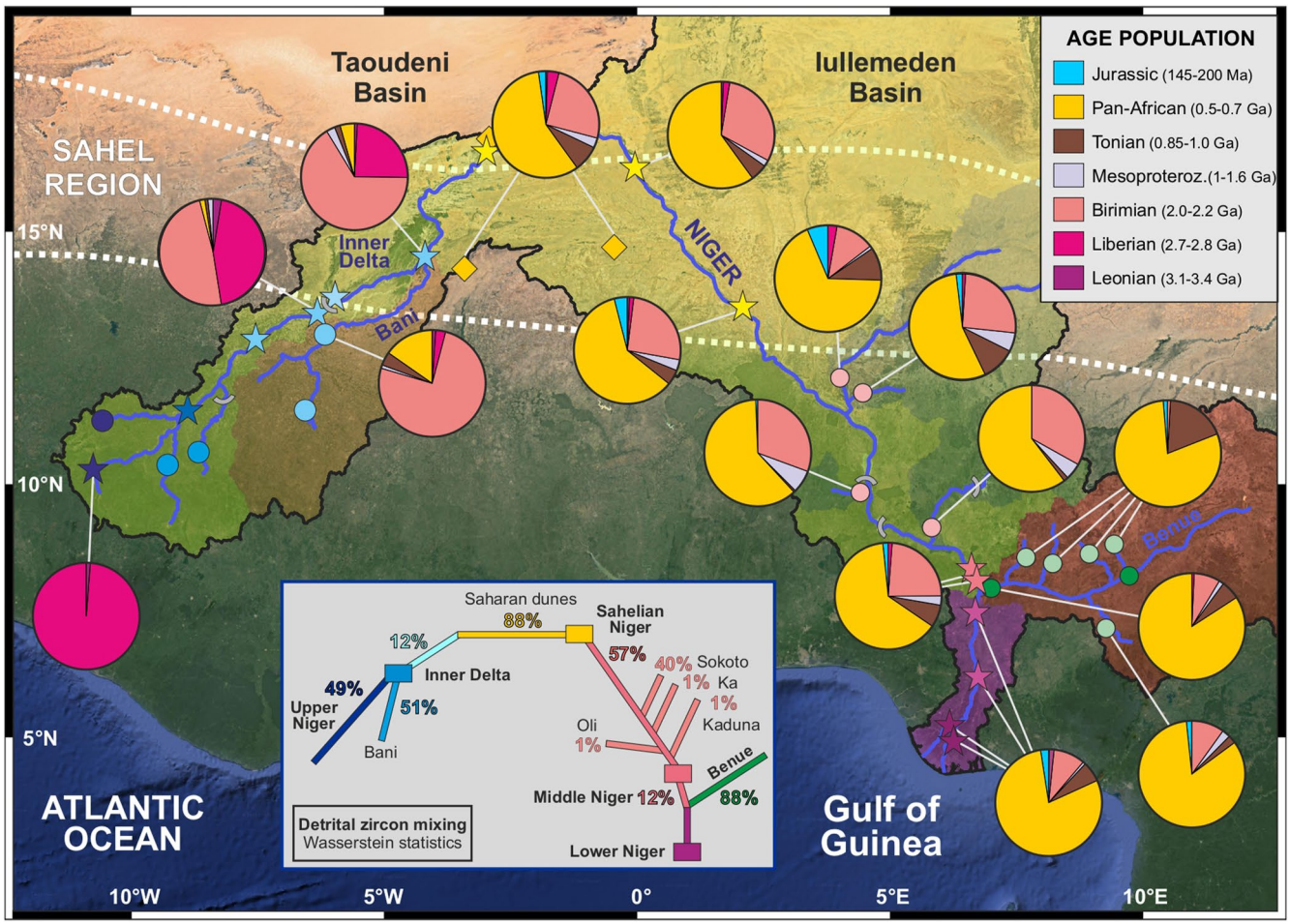

Figure 8. Evolution of the zircon-age signal along the segmented Niger sediment-routing system and zircon-provenance budget (inset). Zircon grains reaching the Inner Delta are derived in subequal proportions from the Upper Niger and Bani rivers, whereas zircon grains reaching the Niger Delta appear to be overwhelmingly supplied by the Benue River.

(McCarthy & Ellery, 1998) and by the Niger River in Mali (Olivry et al., 1994). The temporaneous or permanent segmentation of a fluvial sediment-transport system implies that detritus generated in the highlands is temporarily or permanently stored in the continental interiors and cannot make it to the ocean. The consequent major impact, not only on sediment budgets but also on sediment composition (Garzanti et al., 2021), must be given due consideration in provenance analysis.

7. Time Structure of Source Rocks

In provenance analysis, the diverse time-structure maps of source rocks obtained from the determination of isotopic ratios in sediments constitute a valuable complement to the description of their lithological structure as obtained by traditional petrographic and mineralogical approaches (Garzanti et al., 2018). As a function of the targeted mineral and isotopic system, each technique reproduces a different age distribution across source areas, thus providing complementary information on their evolution through successive episodes of crustal growth. The age map based on U-Pb zircon dating, which provides an overview of igneous and metamorphic crystallization ages, is here complemented with two maps based instead on mantle extraction ages (i.e., on the inferred time of separation of continental crust from the mantle based on a geochemical model of the evolving crust-mantle system) calculated from Sm-Nd and Lu-Hf isotopic ratios (Figure 9).

The West African Craton drained by the Niger River contains three main geological domains: the Archean (Leonian-Liberian) Man Shield, the middle Paleoproterozoic (Eburnean) Leo Shield (Baoulé-Mossi domain), and

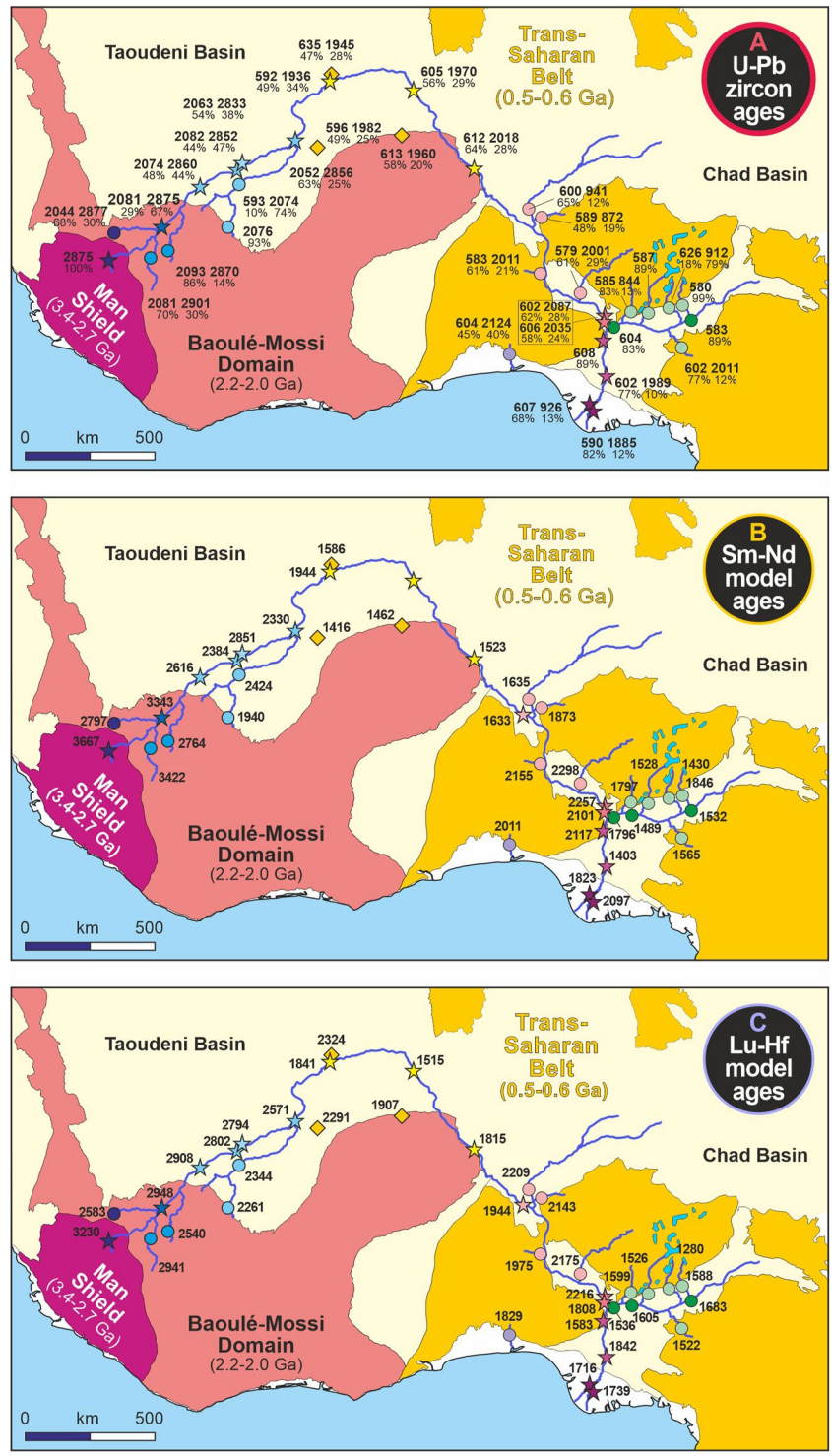

Figure 9. Time-structure maps of the Niger catchment. (a) Along the Upper Niger, Archean zircons from the Man Shield are rapidly diluted by Paleoproterozoic zircons from the Baoulé-Mossi domain. Neoproterozoic zircons are invariably dominant downstream of the Inner Delta. (b, c) $T_{Nd,DM}$ and $T_{Hf,DM}$ model ages, as old as late Eoarchean/Paleoarchean in uppermost Niger sand, decrease progressively to earliest Proterozoic/latest Archean in the Inner Delta and next abruptly to mid-Proterozoic in the Sahelian Niger. In Nigeria, they increase again downstream the Middle Niger, decrease below the Benue confluence, and finally increase in the Niger Delta.

Table 4
Compilation of Geochronological (U-Pb, Rb-Sr, Sm-Nd, and K-Ar) Ages of Igneous and Metamorphic Rocks Exposed in Diverse Domains of the West African Craton

Geological domain	Jurassic	2σ	Pan-African	2σ	Tonian	2σ	Birimian	2σ	Liberian	2σ	Leonian	2σ
Kénéma—Man									2818	*95*	3459	*124*
									75%		*25%*	
Kayes Inlier							2114	*33*				
							100%					
Kedougou-Kéniéba							2109	*40*				
							100%					
Baoulé Mossi							2135	*38*				
							100%					
Dahomeyde Belt			608	*31*	917	*111*	2042	*134*				
			78%		*5%*		*17%*					
N Nigeria basement	184	*39*	615	*66*	780	*28*			2883	*184*	3617	*57*
	31%		*56%*						*7%*		*5%*	
SW Nigeria basement			605	*57*			2038	*206*	2563	*125*		
			67%				*17%*		*17%*			
Adamawa Yadé			607	*36*			2282	*252*				
			92%				*8%*					
Hawal Massif			601	*39*			2105	*157*				
			47%				*53%*					

Note. For each domain, central age, standard deviation, and proportions (italic values) were calculated with *IsoplotR 5.3* (Vermeesch, 2018), implementing the discrete mixture modeling algorithms of Galbraith and Laslett (1993). Full data set of 496 ages from 107 literature sources and information on adopted methods and references are provided in Appendix S3 in Supporting Information S1.

the Neoproterozoic (Pan-African) Trans-Saharan Belt (Table 4). The distribution of zircon-crystallization ages and bulk-sediment model ages in sediment derived from these three main protosources and transported across the Niger drainage basin are highlighted below.

7.1. Archean Protosources

Zircon grains eroded from basement rocks of the Man Shield mostly crystallized during the Liberian episode of crustal growth and yielded an average sample age of 2877 ± 11 Ma. A subordinate number of zircons yielded older Leonian ages (average sample age 3203 ± 19 Ma) (Table 2). Archean zircons represent the entire population in headwater Niger sand and are progressively diluted downstream by zircon grains supplied by younger Proterozoic rocks all along the Niger sediment-routing system. Downstream of the Inner Delta, Leonian zircons show up only sporadically in Saharan dunes but are traced in a very minor amount as far as the Niger Delta (Table 2). Liberian zircons are significant in Saharan dunes and in the sand of the Sahelian Niger and the Sokoto tributary of the Middle Niger, but they show up downstream only in the Niger Delta. It is noteworthy that a minor population of younger, late Neoarchean zircons, occurring in Saharan dunes, Sahelian Niger, and Sokoto tributary sands, also shows up again in the Lower Niger and Niger Delta. Because Archean zircons are negligible throughout the Benue catchment, the reappearance of a few but significant Leonian, Liberian, and late Neoarchean zircons in the Niger Delta indicates reworking of sediment deposited along the coastal plain at earlier times of presumably wetter climate, when neither natural nor artificial efficient barriers to the sediment flux existed along the entire Niger sediment-routing system from Guinea headwaters to the ocean.

7.2. Paleoproterozoic Protosources

Zircon grains eroded from igneous and metamorphic rocks of the Baoulé-Bossi domain crystallized during the Eburnean (Birimian) episode of crustal growth and yielded an average sample age of 2072 ± 14 Ma).

Orosirian-Rhyacian zircons, predominant in all studied tributaries of the Upper Niger and Bani rivers, decrease sharply in abundance downstream of the Inner Delta but remain common in the Sahelian Niger and Middle Niger tributaries, and are most common in Ogun sand derived from the SW Nigeria basement. Instead, Paleoproterozoic zircons are minor in Benue sand, and particularly rare in the sand of its northern tributaries draining the eastern part of the North Nigeria basement, scarcely affected by the Paleoproterozoic orogenic event (Figure 1). As for Archean zircons, also middle Paleoproterozoic zircons increase along the Lower Niger and are significant in Niger Delta distributaries, confirming that the sand generated in the upper parts of the Niger catchment and deposited at earlier times is being extensively reworked across the delta plain. This trend is confirmed by isotope values, which become more negative in fine to medium sand of the Lower Niger and Niger Delta distributaries (ε_{Nd} from −11.6 to −18.4 and ε_{Hf} from −22.3 to −25.5; Table 1).

7.3. Neoproterozoic Protosources

Late Neoproterozoic zircons (Ediacaran peak at 597 ± 13 Ma) first appear in Upper Niger sand as the river enters the Taoudeni Basin in Mali and invariably prevail in Sahelian Niger, Middle Niger, and Lower Niger sands. Neoproterozoic zircons shed by the Pan-African Trans-Saharan Belt are overwhelming throughout the Benue catchment, Ediacaran ages being dominant except for Dep sand where zircon grains are mostly older (Tonian; 912 ± 12 Ma). Although invariably subordinate, zircons of Tonian age (878 ± 34 Ma) widely occur in the Niger catchment from the Sahara to the Niger Delta and are sporadically detected even in the Upper Niger catchment (Tinkisso and Bani sands; Table 2). These data reflect extensive Pan-African metamorphic recrystallization of Archean gneisses and Paleoproterozoic schists representing the core of the Nigeria basement complex, and widespread intrusion of the "Older granites" during growth of the Trans-Saharan Belt.

In the Pan-African domain, from the Sahara to the Niger Delta, $T_{Nd,DM}$ model ages range from Paleoproterozoic (Orosirian-Rhyacian) to early Mesoproterozoic (Calymmian) and $T_{Nd,CHUR}$ model ages from Paleoproterozoic (late Orosirian) to earliest Neoproterozoic (early Tonian). $T_{Hf,DM}$ and $T_{Hf,CHUR}$ model ages are mid-Paleoproterozoic (Orosirian-Rhyacian) for Middle Niger sand, Mesoproterozoic (early Calymmian) for Benue sand, and intermediate (late Paleoproterozoic) for Lower Niger and delta distributary sands. All model ages increase progressively along the Middle Niger, reflecting sediment supply from tributaries draining the western part of the Nigeria basement complex, decrease abruptly downstream of the Benue confluence, indicating overwhelming supply from the Benue River, but increase again in the Niger Delta. This is a further indication of extensive reworking across the delta plain of older sediments generated in larger proportions than today in the Niger catchment upstream of the Benue confluence.

7.4. Other Protosources

Subordinate Mesoproterozoic protosources are indicated by a minor early Calymmian cluster of zircon ages (1576 ± 35 Ma) showing up in the sand of the Inner Delta, Saharan dunes, Middle Niger tributaries, and a few Benue tributaries (Dep and Katsina-Ala; Table 2). Early Calymmian magmatism is in fact reported across the study area, from the Leo Shield in Burkina Faso (Baratoux et al., 2016) to southeastern Nigeria (Ukwang et al., 2012).

Zircons younger than 500 Ma do not occur in the Upper Niger but are present in Saharan dunes and Sahelian Niger, where Permian-Carboniferous to Jurassic zircons become significant (Table 2). Jurassic zircons derived from the "Younger granites" widely exposed in the Jos Plateau occur in sand of the Middle Niger and of its tributaries (their absence in Kaduna sand may be explained by sequestration in the Shiroro reservoir), of the Benue River and of most of its tributaries, and of the Lower Niger as far as the Niger Delta. Cretaceous/Eocene zircons were detected in a few tributaries (Ka, Katsina-Ala), in the Lower Niger, and in the Niger Delta, where a few zircons as young as the Pleistocene reflect recent eruptive events along the Cameroon Line.

8. Conclusions

In Upper Niger sand, U-Pb detrital-zircon ages are exclusively Archean in Guinea headwaters draining the Man Shield (all ages >2.65 Ga, peak at ~2.88 Ga) and dominantly Paleoproterozoic (peak at ~2.07 Ga) in the Inner Delta in Mali, testifying to the progressive downstream dilution by sediment supplied by tributaries draining the Paleoproterozoic Birimian domain. Pan-African ages first appear as the Niger River cuts across Neoproterozoic strata of the Taoudeni Basin. The zircon-age signal changes drastically to dominant Neoproterozoic downstream

of the Inner Delta and becomes indistinguishable from that of Saharan eolian dunes across the Sahel (peak at ~0.6 Ga). An abrupt change is observed also for ε_{Nd} values, which become significantly less negative in the Sahelian Niger than in the Upper Niger and Bani rivers especially for sand but also for clay. Because of hampered flow as the Niger River enters the dune-covered arid lowlands of the Taoudeni Basin, Inner Delta marshlands do not trap only most of the sand generated in Guinea and SW Mali headwaters, but a large part of silt and clay as well. Downstream across the Sahel, sediment load is progressively reconstituted by extensive recycling of dune sand with a late Neoproterozoic zircon-age signature and by eolian dust with less negative ε_{Nd}.

Neoproterozoic zircons supplied in abundance by tributaries draining the Pan-African Trans-Saharan Belt remain dominant throughout Nigeria. Downstream of the Benue confluence, Lower Niger sand yielded very few Paleoproterozoic and no Archean zircons, as in Benue sand, indicating overwhelming supply from the Benue tributary. In the Niger Delta, however, small populations of Paleoarchean (Leonian), Mesoarchean (Liberian) and late Neoarchean zircon reappear, and both ε_{Nd} and ε_{Hf} values become more negative. This indicates extensive reworking of sand deposited along the coastal plain at earlier times of presumably wetter climate, when neither artificial nor major natural barriers to the sand flux existed along the entire Niger River from Guinean headwaters to the ocean.

After the extensive worldwide construction of large dams in the last century, the segmentation of fluvial sediment transport has become the rule for most modern river systems, although this is by no means an exclusively artificial phenomenon. In anorogenic settings, very efficient natural barriers to sediment transport include rift-related lakes as well as vast marshlands formed in subsident regions of the cratonic interiors, such as the Inner Delta in Mali or the Sudd marshes formed by the White Nile in South Sudan. These temporary or even permanent barriers prevent a large part of the detritus generated in the highlands from reaching the ocean, with consequent impact on both sediment budgets and sediment composition, a further unknown that must be given due consideration when solving the complex system of equations called provenance analysis.

Data Availability Statement

Information and data associated with this study are provided in four appendices and in the Google-Earth™ map of sampling sites *NigerDZ.kmz* and archived in the public repository Zenodo (Pastore et al. (2023), https://doi.org/10.5281/zenodo.8424680). Appendix S1 in Supporting Information S1 includes information on sampling sites (Table S1 in Supporting Information S2), bulk-sand petrography, heavy-mineral and geochemical data (Table S2 in Supporting Information S2), and grain-size distribution of zircon grains (Table S3 in Supporting Information S2). Appendix S2 in Supporting Information S1 contains the complete U-Pb detrital-zircon geochronology data set. Appendix S3 in Supporting Information S1 presents a compilation from diverse literature sources of radiometric ages on igneous and metamorphic rocks belonging to the diverse crustal domains exposed in the areas described in this article. Appendix S4 in Supporting Information S1 contains the explanatory captions.

Acknowledgments
Sediment sampling in Guinea and Mali was financed and coordinated by IRD-Bamako and carried out with the fundamental help of Boubacar Baïlo Diakité and Diarra Diallo of the National Hydraulic Directorate of Conakry (DNH-Guinea) and of Boubacar Sidibé and Adama Mariko of the National Hydraulic Directorate of Bamako (DNH-Mali). Other samples in Mali and Niger were collected by Luca Baglioni (student at the University of Milano-Bicocca) and Ibrahim Mamadou (Ph. D student at the Abdou Moumouni at Nyamei and Paris 1 universities). Samples in Nigeria were collected by geology students, professionals, and researchers at the Federal University of Petroleum Resources Effurun (Ilo David Adeyemi, Ogefere Onoharigho, Igbinosa Osaze Temple, Solomon Awakessien, Efenudu Benjamin), Nasarawa State University (Christabel Otite), and University of Lagos (Olusegun Adeaga).

References

Abubakar, M. B. (2014). Petroleum potentials of the Nigerian Benue Trough and Anambra Basin: A regional synthesis. *Natural Resources*, *5*(01), 25–58. https://doi.org/10.4236/nr.2014.51005

Adegoke, O. S., Oyebamiji, A. S., Edet, J. J., Osterloff, P. L., & Ulu, O. K. (2017). Geology of the Niger Delta Basin. In *Cenozoic foraminifera and calcareous nannofossil biostratigraphy of the Niger delta* (Vol. 2, pp. 25–66). Elsevier.

Affaton, P., Kröner, A., & Seddoh, K. F. (2000). Pan-African granulite formation in the Kabye Massif of northern Togo (West Africa): Pb− Pb zircon ages. *International Journal of Earth Sciences*, *88*(4), 778–790. https://doi.org/10.1007/s005310050305

Affaton, P., Rahaman, M. A., Trompette, R., & Sougy, J. (1991). The Dahomeyide Orogen: Tectonothermal evolution and relationships with the Volta Basin. *The West African Orogens and Circum-Atlantic Correlatives*, 107–122. https://doi.org/10.1007/978-3-642-84153-8_6

Allen, J. R. L. (1965). Late Quaternary Niger delta, and adjacent areas: Sedimentary environments and lithofacies. *American Association of Petroleum Geologists Bulletin*, *49*(5), 547–600. https://doi.org/10.1306/a663363a-16c0-11d7-8645000102c1865d

Andersen, T., & Elburg, M. A. (2022). Open-system behaviour of detrital zircon during weathering: An example from the Palaeoproterozoic Pretoria Group, South Africa. *Geological Magazine*, *159*(4), 561–576. https://doi.org/10.1017/s001675682100114x

Andersen, T., Elburg, M. A., & Magwaza, B. N. (2019). Sources of bias in detrital zircon geochronology: Discordance, concealed lead loss and common lead correction. *Earth-Science Reviews*, *197*, 102899. https://doi.org/10.1016/j.earscirev.2019.102899

Anthony, E. J. (2015). Wave influence in the construction, shaping and destruction of river deltas: A review. *Marine Geology*, *361*, 53–78. https://doi.org/10.1016/j.margeo.2014.12.004

Assine, M. L., Merino, E. R., Pupim, F. N., Warren, L. V., Guerreiro, R. L., & McGlue, M. M. (2015). Geology and geomorphology of the Pantanal Basin. In I. Bergier, & M. Assine (Eds.), *Dynamics of the Pantanal Wetland in South America*, *The handbook of environmental chemistry* (Vol. 37, pp. 23–50). Springer.

Attoh, K., Dallmeyer, R. D., & Affaton, P. (1997). Chronology of nappe assembly in the Pan-African Dahomeyide orogen, West Africa: Evidence from $^{40}Ar^{39}Ar$ mineral ages. *Precambrian Research*, *82*(1–2), 153–171. https://doi.org/10.1016/s0301-9268(96)00031-9

Baratoux, L., Jessell, M. W., Söderlund, U., Ernst, R. E., Benoit, M., Naba, S., et al. (2016). Distribution and U-Pb ages of newly recognized regional-scale dyke swarms of the Leo Man Craton. *Acta Geologica Sinica*, *90*(1), 29. https://doi.org/10.1111/1755-6724.12864

Barth, M. G., Rudnick, R. L., Carlson, R. W., Horn, I., & McDonough, W. F. (2002). Re Os and U Pb geochronological constraints on the eclogite–tonalite connection in the Archean Man Shield, West Africa. *Precambrian Research*, *118*(3–4), 267–283. https://doi.org/10.1016/s0301-9268(02)00111-0

Bayon, G., Barrat, J. A., Etoubleau, J., Benoit, M., Bollinger, C., & Révillon, S. (2009). Determination of rare earth elements, Sc, Y, Zr, Ba, Hf, and Th in geological samples by ICP-MS after Tm addition and alkaline fusion. *Geostandards and Geoanalytical Research*, *33*(1), 51–62. https://doi.org/10.1111/j.1751-908x.2008.00880.x

Bea, F., Montero, P., Molina, J. F., Scarrow, J. H., Cambeses, A., & Moreno, J. A. (2018). Lu-Hf ratios of crustal rocks and their bearing on zircon Hf isotope model ages: The effects of accessories. *Chemical Geology*, *484*, 179–190. https://doi.org/10.1016/j.chemgeo.2017.11.034

Bea, F., Montero, P., & Ortega, M. (2006). A LA–ICP–MS evaluation of Zr reservoirs in common crustal rocks: Implications for Zr and Hf geochemistry, and zircon-forming processes. *The Canadian Mineralogist*, *44*(3), 693–714. https://doi.org/10.2113/gscanmin.44.3.693

Blichert-Toft, J., Chauvel, C., & Albarède, F. (1997). Separation of Hf and Lu for high-precision isotope analysis of rock samples by magnetic sector-multiple collector ICP-MS. *Contributions to Mineralogy and Petrology*, *127*(3), 248–260. https://doi.org/10.1007/s004100050278

Blichert-Toft, J., & Puchtel, I. S. (2010). Depleted mantle sources through time: Evidence from Lu–Hf and Sm–Nd isotope systematics of Archean komatiites. *Earth and Planetary Science Letters*, *297*(3–4), 598–606. https://doi.org/10.1016/j.epsl.2010.07.012

Bouvier, A., Vervoort, J. D., & Patchett, P. J. (2008). The Lu–Hf and Sm–Nd isotopic composition of CHUR: Constraints from unequilibrated chondrites and implications for the bulk composition of terrestrial planets. *Earth and Planetary Science Letters*, *273*(1–2), 48–57. https://doi.org/10.1016/j.epsl.2008.06.010

Bouyo, M. H., Zhao, Y., Penaye, J., Zhang, S. H., & Njel, U. O. (2015). Neoproterozoic subduction-related metavolcanic and metasedimentary rocks from the Rey Bouba Greenstone Belt of north-central Cameroon in the Central African Fold Belt: New insights into a continental arc geodynamic setting. *Precambrian Research*, *261*, 40–53. https://doi.org/10.1016/j.precamres.2015.01.012

Bowden, P., & Kinnaird, J. A. (1984). The petrology and geochemistry of alkaline granites from Nigeria. *Physics of the Earth and Planetary Interiors*, *35*(1–3), 199–211. https://doi.org/10.1016/0031-9201(84)90043-8

Breiter, K., Lamarão, C. N., Borges, R. M. K., & Dall'Agnol, R. (2014). Chemical characteristics of zircon from A-type granites and comparison to zircon of S-type granites. *Lithos*, *192*, 208–225. https://doi.org/10.1016/j.lithos.2014.02.004

Bruguier, O., Dada, S., & Lancelot, J. R. (1994). Early Archaean component (>3.5 Ga) within a 3.05 Ga orthogneiss from northern Nigeria: U-Pb zircon evidence. *Earth and Planetary Science Letters*, *125*(1–4), 89–103. https://doi.org/10.1016/0012-821x(94)90208-9

Burke, K., Dessauvagie, T. F. J., & Whiteman, A. J. (1971). Opening of the Gulf of Guinea and geological history of the Benue Depression and Niger delta. *Nature Physical Science*, *233*(38), 51–55. https://doi.org/10.1038/physci233051a0

Bute, S. I., Yang, X. Y., Cao, J., Liu, L., Deng, J. H., Vela Haruna, I. V., et al. (2020). Origin and tectonic implications of ferroan alkali-calcic granitoids from the Hawal Massif, east-eastern Nigeria terrane: Clues from geochemistry and zircon U-Pb-Hf isotopes. *International Geology Review*, *62*(2), 129–152. https://doi.org/10.1080/00206814.2019.1593250

Caby, R. (1987). The Pan-African belt of West Africa from the Sahara desert to the Gulf of Benin. *Anatomy of Mountain Ranges*, *1*, 129–170.

Caby, R., & Boesse, J. M. (2001). Pan-African nappe system in southwest Nigeria: The Ife-Ilesha schist belt. *Journal of African Earth Sciences*, *33*(2), 211–225. https://doi.org/10.1016/s0899-5362(01)80060-9

Caracciolo, L. (2020). Sediment generation and sediment routing systems from a quantitative provenance analysis perspective: Review, application and future development. *Earth-Science Reviews*, *209*, 103226. https://doi.org/10.1016/j.earscirev.2020.103226

Chew, D., O'Sullivan, G., Caracciolo, L., Mark, C., & Tyrrell, S. (2020). Sourcing the sand: Accessory mineral fertility, analytical and other biases in detrital U-Pb provenance analysis. *Earth-Science Reviews*, *202*, 103093. https://doi.org/10.1016/j.earscirev.2020.103093

Chu, N. C., Taylor, R. N., Chavagnac, V., Nesbitt, R. W., Boella, R. M., Milton, J. A., et al. (2002). Hf isotope ratio analysis using multi-collector inductively coupled plasma mass spectrometry: An evaluation of isobaric interference corrections. *Journal of Analytical Atomic Spectrometry*, *17*(12), 1567–1574. https://doi.org/10.1039/b206707b

Coleman, J. M., Huh, O. K., & Braud, D. (2008). Wetland loss in world deltas. *Journal of Coastal Research*, *24*(10024), 1–14. https://doi.org/10.2112/05-0607.1

Daramola, J., Adepehin, E. J., Ekhwan, T. M., Choy, L. K., Mokhtar, J., & Tabiti, T. S. (2022). Impacts of land-use change, associated land-use area and runoff on watershed sediment yield: Implications from the Kaduna Watershed. *Water*, *14*(3), 325. https://doi.org/10.3390/w14030325

Dawaï, D., Bouchez, J. L., Paquette, J. L., & Tchameni, R. (2013). The Pan-African quartz-syenite of Guider (north-Cameroon): Magnetic fabric and U–Pb dating of a late-orogenic emplacement. *Precambrian Research*, *236*, 132–144. https://doi.org/10.1016/j.precamres.2013.07.008

Deckart, K., Bertrand, H., & Liégeois, J. P. (2005). Geochemistry and Sr, Nd, Pb isotopic composition of the central Atlantic magmatic province (CAMP) in Guyana and Guinea. *Lithos*, *82*(3–4), 289–314. https://doi.org/10.1016/j.lithos.2004.09.023

Deer, W. A., Howie, R. A., & Zussman, J. (1997). *Rock-forming minerals* (Vol. 1–5). Geological Society of London.

De Paolo, D. J. (1981). Neodymium isotopes in the Colorado Front Range and crust–mantle evolution in the Proterozoic. *Nature*, *291*(5812), 193–196. https://doi.org/10.1038/291193a0

DePaolo, D. J., Linn, A. M., & Schubert, G. (1991). The continental crustal age distribution: Methods of determining mantle separation ages from Sm-Nd isotopic data and application to the southwestern United States. *Journal of Geophysical Research*, *96*(B2), 2071–2088. https://doi.org/10.1029/90jb02219

Deynoux, M., Affaton, P., Trompette, R., & Villeneuve, M. (2006). Pan-African tectonic evolution and glacial events registered in Neoproterozoic to Cambrian cratonic and foreland basins of West Africa. *Journal of African Earth Sciences*, *46*(5), 397–426. https://doi.org/10.1016/j.jafrearsci.2006.08.005

Egal, E., Thiéblemont, D., Lahondere, D., Guerrot, C., Costea, C. A., Iliescu, D., et al. (2002). Late Eburnean granitization and tectonics along the western and northwestern margin of the Archean Kénéma–Man domain (Guinea, West African Craton). *Precambrian Research*, *117*(1–2), 57–84. https://doi.org/10.1016/s0301-9268(02)00060-8

Elatikpo, S. M., Li, H., Zheng, H., Girei, M. B., Wu, J., & Amuda, A. K. (2022). Cryogenian crustal evolution in western Nigeria shield: Whole-rock geochemistry, Sr-Nd, and zircon U-Pb-Hf isotopic evidence from Bakoshi-Gadanya granites. *International Geology Review*, *64*(18), 2626–2652. https://doi.org/10.1080/00206814.2021.1998799

Fairhead, J. D., Green, C. M., Masterton, S. M., & Guiraud, R. (2013). The role that plate tectonics, inferred stress changes and stratigraphic unconformities have on the evolution of the West and Central African Rift System and the Atlantic continental margins. *Tectonophysics*, *594*, 118–127. https://doi.org/10.1016/j.tecto.2013.03.021

FAO and IHE Delft (2020). Water accounting in the Niger River Basin. FAO WaPOR water accounting reports, *120*. https://doi.org/10.4060/cb1274en

Ferré, E., Déléris, J., Bouchez, J. L., Lar, A. U., & Peucat, J. J. (1996). The Pan-African reactivation of Eburnean and Archaean provinces in Nigeria: Structural and isotopic data. *Journal of the Geological Society*, *153*(5), 719–728. https://doi.org/10.1144/gsjgs.153.5.0719

Ferré, E., Gleizes, G., & Caby, R. (2002). Obliquely convergent tectonics and granite emplacement in the Trans-Saharan belt of Eastern Nigeria: A synthesis. *Precambrian Research*, *114*(3–4), 199–219. https://doi.org/10.1016/s0301-9268(01)00226-1

Ferry, L., Muther, N., Coulibaly, N., Martin, D., Mietton, M., Coulibaly, Y. C., et al. (2012). *Le fleuve Niger, de la forêt tropicale guinéenne au désert saharien: Les grands traits des régimes hydrologiques*. Mémoire IRD & UNESCO. Retrieved from https://unesdoc.unesco.org/ark:/48223/pf0000215565

Fitches, W. R., Ajibade, A. C., Egbuniwe, I. G., Holt, R. W., & Wright, J. B. (1985). Late Proterozoic schist belts and plutonism in NW Nigeria. *Journal of the Geological Society London*, *142*(2), 319–337. https://doi.org/10.1144/gsjgs.142.2.0319

Folk, R. L., & Ward, W. C. (1957). Brazos River bar; a study in the significance of grain size parameters. *Journal of Sedimentary Petrology*, *27*(1), 3–26. https://doi.org/10.1306/74d70646-2b21-11d7-8648000102c1865d

Galbraith, R. F., & Laslett, G. M. (1993). Statistical models for mixed fission track ages. *Nuclear Tracks and Radiation Measurements*, *21*(4), 459–470. https://doi.org/10.1016/1359-0189(93)90185-c

Ganade, C. E., Cordani, U. G., Agbossoumounde, Y., Caby, R., Basei, M. A., Weinberg, R. F., & Sato, K. (2016). Tightening-up NE Brazil and NW Africa connections: New U–Pb/Lu–Hf zircon data of a complete plate tectonic cycle in the Dahomey belt of the West Gondwana Orogen in Togo and Benin. *Precambrian Research*, *276*, 24–42. https://doi.org/10.1016/j.precamres.2016.01.032

Garçon, M. (2021). Episodic growth of felsic continents in the past 3.7 Ga. *Science Advances*, *7*(39), eabj1807. https://doi.org/10.1126/sciadv.abj1807

Garzanti, E. (2016). From static to dynamic provenance analysis—Sedimentary petrology upgraded. *Sedimentary Geology*, *336*, 3–13. https://doi.org/10.1016/j.sedgeo.2015.07.010

Garzanti, E. (2019). Petrographic classification of sand and sandstone. *Earth-Science Reviews*, *192*, 545–563. https://doi.org/10.1016/j.earscirev.2018.12.014

Garzanti, E., & Andò, S. (2007). Plate tectonics and heavy-mineral suites of modern sands. In M. A. Mange, & D. T. Wright (Eds.), *Heavy minerals in use*, *Developments in sedimentology series* (Vol. 58, pp. 741–763). Elsevier.

Garzanti, E., & Andò, S. (2019). Heavy minerals for junior woodchucks. *Minerals*, *9*(3), 148. https://doi.org/10.3390/min9030148

Garzanti, E., Andò, S., France-Lanord, C., Vezzoli, G., Censi, P., Galy, V., & Najman, Y. (2010). Mineralogical and chemical variability of fluvial sediments: 1. Bedload sand (Ganga–Brahmaputra, Bangladesh). *Earth and Planetary Science Letters*, *299*(3–4), 368–381. https://doi.org/10.1016/j.epsl.2010.09.017

Garzanti, E., Andò, S., Padoan, M., Vezzoli, G., & El Kammar, A. (2015). The modern Nile sediment system: Processes and products. *Quaternary Science Reviews*, *130*, 9–56. https://doi.org/10.1016/j.quascirev.2015.07.011

Garzanti, E., Andò, S., & Vezzoli, G. (2008). Settling equivalence of detrital minerals and grain-size dependence of sediment composition. *Earth and Planetary Science Letters*, *273*(1–2), 138–151. https://doi.org/10.1016/j.epsl.2008.06.020

Garzanti, E., Bayon, G., Dinis, P., Vermeesch, P., Pastore, G., Resentini, A., et al. (2022). The segmented Zambezi sedimentary system from source to sink: 2. Geochemistry, clay minerals, and detrital geochronology. *The Journal of Geology*, *130*(3), 171–208. https://doi.org/10.1086/719166

Garzanti, E., Bayon, G., Vermeesch, P., Barbarano, M., Pastore, G., Resentini, A., et al. (2022). The Zambezi deep-sea fan: Mineralogical, REE, Zr/Hf, Nd-isotope, and zircon-age variability in feldspar-rich passive-margin turbidites. *Journal of Sedimentary Research*, *92*(11), 1022–1043. https://doi.org/10.2110/jsr.2022.033

Garzanti, E., Pastore, G., Resentini, A., Vezzoli, G., Vermeesch, P., Ncube, L., et al. (2021). The segmented Zambezi sedimentary system from source to sink: 1. Sand petrology and heavy minerals. *The Journal of Geology*, *129*(4), 343–369. https://doi.org/10.1086/715792

Garzanti, E., Resentini, A., Vezzoli, G., Andò, S., Malusà, M., & Padoan, M. (2012). Forward compositional modelling of Alpine orogenic sediments. *Sedimentary Geology*, *280*, 149–164. https://doi.org/10.1016/j.sedgeo.2012.03.012

Garzanti, E., Vermeesch, P., Rittner, M., & Simmons, M. (2018). The zircon story of the Nile: Time-structure maps of source rocks and discontinuous propagation of detrital signals. *Basin Research*, *30*(6), 1098–1117. https://doi.org/10.1111/bre.12293

Garzanti, E., Vermeesch, P., Vezzoli, G., Andò, S., Botti, E., Limonta, M., et al. (2019). Congo River sand and the equatorial quartz factory. *Earth-Science Reviews*, *197*, 102918. https://doi.org/10.1016/j.earscirev.2019.102918

Glodji, C. L. A. (2012). La zone de cisaillement de Kandi et le magmatisme associé dans la région de Savalou-Dassa (Bénin): étude structurale, pétrologique et géochronologique. Doctoral dissertation (p. 260).

Goldstein, S. L., Arndt, N. T., & Stallard, R. F. (1997). The history of a continent from U-Pb ages of zircons from Orinoco River sand and Sm-Nd isotopes in Orinoco basin river sediments. *Chemical Geology*, *139*(1–4), 271–286. https://doi.org/10.1016/s0009-2541(97)00039-9

Goodenough, K. M., Lusty, P. A. J., Roberts, N. M. W., Key, R. M., & Garba, A. (2014). Post-collisional Pan-African granitoids and rare metal pegmatites in western Nigeria: Age, petrogenesis, and the 'pegmatite conundrum'. *Lithos*, *200*, 22–34. https://doi.org/10.1016/j.lithos.2014.04.006

Grant, N. K., Rex, D. C., & Freeth, S. J. (1972). Potassium-argon ages and strontium isotope ratio measurements from volcanic rocks in northeastern Nigeria. *Contributions to Mineralogy and Petrology*, *35*(4), 277–292. https://doi.org/10.1007/bf00371310

Greensfelder, L. (2002). Subtleties of sand reveal how mountains crumble. *Science*, *295*(5553), 256–258. https://doi.org/10.1126/science.295.5553.256

Grenholm, M., Jessell, M., & Thébaud, N. (2019). A geodynamic model for the Paleoproterozoic (ca. 2.27–1.96 Ga) Birimian Orogen of the southern West African Craton–Insights into an evolving accretionary-collisional orogenic system. *Earth-Science Reviews*, *192*, 138–193. https://doi.org/10.1016/j.earscirev.2019.02.006

Griffin, W. L., Powell, W. J., Pearson, N. J., & O'Reilly, S. Y. (2008). GLITTER: Data reduction software for laser ablation ICP-MS. In P. Sylvester (Ed.), *Laser ablation-ICP-MS in the Earth sciences: Current practices and outstanding issues: Mineralogical association of Canada*, *Short course series* (Vol. 40, pp. 204–207).

Guo, R., Hu, X., Garzanti, E., Lai, W., Yan, B., & Mark, C. (2020). How faithfully do the geochronological and geochemical signatures of detrital zircon, titanite, rutile and monazite record magmatic and metamorphic events? A case study from the Himalaya and Tibet. *Earth-Science Reviews*, *201*, 103082. https://doi.org/10.1016/j.earscirev.2020.103082

Hay, W. W. (1998). Detrital sediment fluxes from continents to oceans. *Chemical Geology*, *145*(3–4), 287–323. https://doi.org/10.1016/s0009-2541(97)00149-6

Hinderer, M. (2001). Late Quaternary denudation of the Alps, valley and lake fillings and modern river loads. *Geodinamica Acta*, *14*(4), 231–263. https://doi.org/10.1080/09853111.2001.11432446

Hinderer, M. (2012). From gullies to mountain belts: A review of sediment budgets at various scales. *Sedimentary Geology*, *280*, 21–59. https://doi.org/10.1016/j.sedgeo.2012.03.009

Ibe, C. U. (2020). Geochemistry of the Precambrian basement of the Bamenda massif of southeastern Nigeria: Petrogenesis and tectonic setting. *Geológica Acta*, *18*, 1–13. https://doi.org/10.1344/GeologicaActa2020.18.19

Ingersoll, R. V., Bullard, T. F., Ford, R. L., Grimm, J. P., Pickle, J. D., & Sares, S. W. (1984). The effect of grain size on detrital modes: A test of the Gazzi-Dickinson point-counting method. *Journal of Sedimentary Petrology*, *54*, 103–116. https://doi.org/10.1306/212f83b9-2b24-11d7-8648000102c1865d

Jackson, S. E., Pearson, N. J., Griffin, W. L., & Belousova, E. A. (2004). The application of laser ablation-inductively coupled plasma-mass spectrometry to in situ U–Pb zircon geochronology. *Chemical Geology*, *211*(1–2), 47–69. https://doi.org/10.1016/j.chemgeo.2004.06.017

Kalsbeek, F., Affaton, P., Ekwueme, B., Frei, R., & Thrane, K. (2012). Geochronology of granitoid and metasedimentary rocks from Togo and Benin, West Africa: Comparisons with NE Brazil. *Precambrian Research*, *196*, 218–233. https://doi.org/10.1016/j.precamres.2011.12.006

Kinny, P. D., & Maas, R. (2003). Lu–Hf and Sm–Nd isotope systems in zircon. In J. M. Hanchar, & P. W. O. Hoskin (Eds.), *Reviews in mineralogy and geochemistry—Zircon* (pp. 327–341). Mineralogical Society of America and Geochemical Society.

Kristinsdóttir, B., Scherstén, A., Kemp, A. I. S., & Petersson, A. (2013). Juvenile crustal growth during the Palaeoproterozoic: U–Pb–O–Hf isotopes from detrital zircon from Ghana. *Mineralogical Magazine*, *77*, 1513.

Kröner, A., Ekwueme, B. N., & Pidgeon, R. T. (2001). The oldest rocks in West Africa: SHRIMP zircon age for early Archean migmatitic orthogneiss at Kaduna, northern Nigeria. *The Journal of Geology*, *109*(3), 399–406. https://doi.org/10.1086/319979

Kuenzer, C., van Beijma, S., Gessner, U., & Dech, S. (2014). Land surface dynamics and environmental challenges of the Niger Delta, Africa: Remote sensing-based analyses spanning three decades (1986–2013). *Applied Geography*, *53*, 354–368. https://doi.org/10.1016/j.apgeog.2014.07.002

Lahondère, D., Thiéblemont, D., Tegyey, M., Guerrot, C., & Diabate, B. (2002). First evidence of early Birimian (2.21 Ga) volcanic activity in Upper Guinea: The volcanics and associated rocks of the Niani suite. *Journal of African Earth Sciences*, *35*(3), 417–431. https://doi.org/10.1016/s0899-5362(02)00145-8

Lebrun, E., Thébaud, N., Miller, J., Ulrich, S., Bourget, J., & Terblanche, O. (2016). Geochronology and lithostratigraphy of the Siguiri district: Implications for gold mineralisation in the Siguiri Basin (Guinea, West Africa). *Precambrian Research*, *274*, 136–160. https://doi.org/10.1016/j.precamres.2015.10.011

Lerouge, C., Feybesse, J. L., Guerrot, C., Billa, M., & Diaby, S. (2004). Reaction textures in Proterozoic calcsilicates from northern Guinea: A record of the fluid evolution. *Journal of African Earth Sciences*, *39*(3–5), 105–113. https://doi.org/10.1016/j.jafrearsci.2004.07.058

L'Hôte, Y., & Mahé, G. (1995). *Carte des précipitations moyennes annuelles en Afrique de l'Ouest et Centrale (période 1951-1989)*. IRD Editions.

Lipp, A., & Vermeesch, P. (2023). Comparing detrital age spectra and other geological distributions using the Wasserstein distance. *Geochronology*, *5*(1), 263–270. https://doi.org/10.5194/gchron-5-263-2023

Ludwig, K. R. (1998). On the treatment of concordant uranium-lead ages. *Geochimica et Cosmochimica Acta*, *62*(4), 665–676. https://doi.org/10.1016/s0016-7037(98)00059-3

Malusà, M. G., Resentini, A., & Garzanti, E. (2016). Hydraulic sorting and mineral fertility bias in detrital geochronology. *Gondwana Research*, *31*, 1–19. https://doi.org/10.1016/j.gr.2015.09.002

McCarthy, T. S., & Ellery, W. N. (1998). The Okavango delta. *Transactions of the Royal Society of South Africa*, *53*(2), 157–182. https://doi.org/10.1080/00359199809520384

Milliman, J. D., & Farnsworth, K. L. (2011). *River discharge to the coastal ocean: A global synthesis* (p. 384). Cambridge University Press.

Najman, Y. (2006). The detrital record of orogenesis: A review of approaches and techniques used in the Himalayan sedimentary basins. *Earth-Science Reviews*, *74*(1–2), 1–72. https://doi.org/10.1016/j.earscirev.2005.04.004

Nasdala, L., Irmer, G., & Wolf, D. (1995). The degree of metamictization in zircon: A Raman spectroscopic study. *European Journal of Mineralogy*, *7*(3), 471–478. https://doi.org/10.1127/ejm/7/3/0471

NEDECO. (1961). *The waters of the Niger delta* (p. 317). Netherlands Engineering Consultants.

Ngako, V., Njonfang, E., Aka, F. T., Affaton, P., & Nnange, J. M. (2006). The North–South Paleozoic to Quaternary trend of alkaline magmatism from Niger–Nigeria to Cameroon: Complex interaction between hotspots and Precambrian faults. *Journal of African Earth Sciences*, *45*(3), 241–256. https://doi.org/10.1016/j.jafrearsci.2006.03.003

Ngoniri, A. H., Tamehe, S. L., Ganno, S., Ngnotue, T., Chen, Z. X., Li, H., et al. (2021). Geochronology and petrogenesis of the Pan-African granitoids from Mbondo-Ngazi Tina in the Adamawa-Yadé Domain, Central Cameroon. *International Journal of Earth Sciences*, *110*(6), 2221–2245. https://doi.org/10.1007/s00531-021-02071-3

Obaje, N. G. (2009). Younger granites. In N. G. Obaje (Ed.), *Geology and mineral resources of Nigeria* (pp. 31–48). Springer.

Obaje, N. G., Bomai, A., Moses, S. D., Ali, M., Aweda, A., Habu, S. J., et al. (2020). Updates on the geology and potential petroleum system of the Bida Basin in Central Nigeria. *Petroleum Science and Engineering*, *4*(1), 23–33. https://doi.org/10.11648/j.pse.20200401.13

Ogezi, A. E. O. (1977). Geochemistry and geochronology of basement rocks from northwestern Nigeria. Doctoral dissertation (p. 295). University of Leeds (Department of Earth Sciences).

Ogunkoya, O. O. (2023). Kainji Dam and Lake. In A. Faniran, L. K. Jeje, O. A. Fashae, & A. O. Olusola (Eds.), *Landscapes and landforms of Nigeria* (pp. 161–174). Springer.

Olivry, J. C. (1995). *Fonctionnement hydrologique de la Cuvette Lacustre du Niger et essai de modélisation de l'inondation du Delta intérieur. Grands bassins fluviaux périatlantiques: Congo, Niger, Amazone* (pp. 267–280). ORSTOM.

Olivry, J. C. (1998). Hydrological and geochemical studies on the Sahelo-Sudanian basin of the Niger river. In C. Causse, & F. Gasse (Eds.), *Symposium international sur l'hydrologie et la geochimie isotopique* (Vol. 1–2, pp. 73–95).

Olivry, J. C., Bricquet, J. P., Bamba, F., & Diara, M. (1995). Le régime hydrologique du Niger supérieur et le déficit des deux dernières décennies. In J. C. Olivry, & J. Boulègue (Eds.), *Grands Bassins Fluviaux Périatlantiques: Congo, Niger, Amazone; Collection Colloque and Séminaire* (pp. 251–266). ORSTOM.

Olivry, J. C., Diallo, I. M., & Bricquet, J. P. (1994). *Quelques données préliminaires sur l'environnement et la qualité des apports du Niger au Sahel* (Vol. 111). ORSTOM, CNRST.

Ominigbo, O. E. (2022). Evolution of the Nigerian basement complex: Current status and suggestions for future research. *Journal of Mining and Geology*, *58*(1), 229–236.

Ominigbo, O. E., Ukwang, E. E., Okumoko, D. P., & Ukpai, U. J. (2020). Petrogenesis and tectonic setting of the basement rocks around Irruan area, Bamenda Massif, SE Nigeria. *Journal of Geosciences and Geomatics*, *8*(1), 35–44.

Oversby, V. M. (1975). Lead isotopic study of aplites from the Precambrian basement rocks near Ibadan, southwestern Nigeria. *Earth and Planetary Science Letters*, *27*(2), 177–180. https://doi.org/10.1016/0012-821x(75)90027-8

Padoan, M., Garzanti, E., Harlavan, Y., & Villa, I. M. (2011). Tracing Nile sediment sources by Sr and Nd isotope signatures (Uganda, Ethiopia, Sudan). *Geochimica et Cosmochimica Acta*, *75*(12), 3627–3644. https://doi.org/10.1016/j.gca.2011.03.042

Parra-Avila, L. A., Belousova, E., Fiorentini, M. L., Baratoux, L., Davis, J., Miller, J., & McCuaig, T. C. (2016). Crustal evolution of the Paleoproterozoic Birimian terranes of the Baoulé-Mossi domain, southern West African Craton: U–Pb and Hf-isotope studies of detrital zircons. *Precambrian Research*, *274*, 25–60. https://doi.org/10.1016/j.precamres.2015.09.005

Parra-Avila, L. A., Kemp, A. I., Fiorentini, M. L., Belousova, E., Baratoux, L., Block, S., et al. (2017). The geochronological evolution of the Paleoproterozoic Baoulé-Mossi domain of the southern West African Craton. *Precambrian Research*, *300*, 1–27. https://doi.org/10.1016/j.precamres.2017.07.036

Pastore, G., Baird, T., Vermeesch, P., Bristow, C., Resentini, A., & Garzanti, E. (2021). Provenance and recycling of Sahara Desert sand. *Earth-Science Reviews*, *216*, 103606. https://doi.org/10.1016/j.earscirev.2021.103606

Pastore, G., Garzanti, E., Vermeesch, P., Bayon, G., Resentini, A., Braquet, N., & Overare, B. (2023). The zircon story of the Niger River: Time-structure maps of the West African Craton and discontinuous propagation of provenance signals across a disconnected sediment-routing system. https://doi.org/10.5281/zenodo.8424680

Pell, S. D., Williams, I. S., & Chivas, A. R. (1997). The use of protolith zircon-age fingerprints in determining the protosource areas for some Australian dune sands. *Sedimentary Geology*, *109*(3–4), 233–260. https://doi.org/10.1016/s0037-0738(96)00061-9

Penaye, J., Toteu, S. F., Michard, A., Bertrand, J. M., & et Dautel, D. (1989). Reliques granulitiques d'âge protérozoïque inférieur dans la zone mobile panafricaine d'Afrique centrale au Cameroun; géochronologie U–Pb sur zircons. *Comptes Rendu de l'Académie des Sciences de Paris*, *309*, 315–318.

Picouet, C., Dupré, B., Orange, D., & Valladon, M. (2002). Major and trace element geochemistry in the upper Niger River (Mali): Physical and chemical weathering rates and CO_2 consumption. *Chemical Geology*, *185*(1–2), 93–124. https://doi.org/10.1016/s0009-2541(01)00398-9

Pidgeon, R. T., Breemen, V., & Mo, O. (1976). Pan African and earlier events in the basement complex of Nigeria. In *25th international geological congress* (Vol. 3, p. 667).

Rahaman, M. A. (1988). Recent advances in the study of the basement complex of Nigeria. Precambrian geology of Nigeria. *Geological Survey of Nigeria*, 11–41.

Rahaman, M. A., Van Breemen, O., Bowden, P., & Bennett, J. N. (1984). Age migrations of anorogenic ring complexes in Northern Nigeria. *The Journal of Geology*, *92*(2), 173–184. https://doi.org/10.1086/628847

Rahaman, M. A. O., Fadiya, S. L., Adekola, S. A., Coker, S. J., Bale, R. B., Olawoki, O. A., et al. (2019). A revised stratigraphy of the Bida Basin, Nigeria. *Journal of African Earth Sciences*, *151*, 67–81. https://doi.org/10.1016/j.jafrearsci.2018.11.016

Resentini, A., Andò, S., Garzanti, E., Malusà, M. G., Pastore, G., Vermeesch, P., et al. (2020). Zircon as a provenance tracer: Coupling Raman spectroscopy and U-Pb geochronology in source-to-sink studies. *Chemical Geology*, *555*, 119828. https://doi.org/10.1016/j.chemgeo.2020.119828

Resentini, A., Goren, L., Castelltort, S., & Garzanti, E. (2017). Partitioning sediment flux by provenance and tracing erosion patterns in Taiwan. *Journal of Geophysical Research: Earth Surface*, *122*(7), 1430–1454. https://doi.org/10.1002/2016jf004026

Rudnick, R. L., & Gao, S. (2003). Composition of the continental crust. In R. L. Rudnick, H. D. Holland, & K. K. Turekian (Eds.), *Treatise on geochemistry. The crust, 3* (pp. 1–64). Elsevier Pergamon.

Samson, S. D., Moecher, D. P., & Satkoski, A. M. (2018). Inherited, enriched, heated, or recycled? Examining potential causes of Earth's most zircon fertile magmatic episode. *Lithos*, *314*, 350–359. https://doi.org/10.1016/j.lithos.2018.06.015

Sláma, J., Košler, J., Condon, D. J., Crowley, J. L., Gerdes, A., Hanchar, J. M., et al. (2008). Plešovice zircon—A new natural reference material for U–Pb and Hf isotopic microanalysis. *Chemical Geology*, *249*(1–2), 1–35. https://doi.org/10.1016/j.chemgeo.2007.11.005

Soba, D., Michard, A., Toteu, S. F., Norman, D. I., Penaye, J., Ngako, V., et al. (1991). Données géochronologiques nouvelles (Rb–Sr, U–Pb, Sm–Nd) sur la zone mobile panafricaine de l'Est Cameroun: âge Protérozoïque supérieur de la série de Lom. *Comptes Rendu de l'Académie des Sciences*, *315*, 1453–1458.

Stanley, D. J., & Warne, A. G. (1998). Nile Delta in its destruction phase. *Journal of Coastal Research*, 795–825.

Sundell, K. E., & Saylor, J. E. (2017). Unmixing detrital geochronology age distributions. *Geochemistry, Geophysics, Geosystems*, *18*(8), 2872–2886. https://doi.org/10.1002/2016gc006774

Syvitski, J. P., Kettner, A. J., Overeem, I., Giosan, L., Brakenridge, G. R., Hannon, M., & Bilham, R. (2013). Anthropocene metamorphosis of the Indus Delta and lower floodplain. *Anthropocene*, *3*, 24–35. https://doi.org/10.1016/j.ancene.2014.02.003

Tanaka, T., Togashi, S., Kamioka, H., Amakawa, H., Kagami, H., Hamamoto, T., et al. (2000). JNdi-1: A neodymium isotopic reference in consistency with LaJolla neodymium. *Chemical Geology*, *168*(3–4), 279–281. https://doi.org/10.1016/s0009-2541(00)00198-4

Taylor, S. R., & Mclennan, S. M. (1995). The geochemical evolution of the continental crust. *Reviews of Geophysics*, *33*(2), 241–265. https://doi.org/10.1029/95rg00262

Thiéblemont, D., Delor, C., Cocherie, A., Lafon, J. M., Goujou, J. C., Baldé, A., et al. (2001). A 3.5 Ga granite–gneiss basement in Guinea: Further evidence for early archean accretion within the West African Craton. *Precambrian Research*, *108*(3–4), 179–194. https://doi.org/10.1016/s0301-9268(00)00160-1

Thiéblemont, D., Goujou, J. C., Egal, E., Cocherie, A., Delor, C., Lafon, J. M., & Fanning, C. M. (2004). Archean evolution of the Leo Rise and its Eburnean reworking. *Journal of African Earth Sciences*, *39*(3–5), 97–104. https://doi.org/10.1016/j.jafrearsci.2004.07.059

Toteu, S. F., Penaye, J., & Djomani, Y. P. (2004). Geodynamic evolution of the Pan-African belt in central Africa with special reference to Cameroon. *Canadian Journal of Earth Sciences*, *41*(1), 73–85. https://doi.org/10.1139/e03-079

Tubosun, I. A., Lancelot, J. R., Rahaman, M. A., & Ocan, O. (1984). U-Pb Pan-African ages of two charnockite-granite associations from Southwestern Nigeria. *Contributions to Mineralogy and Petrology*, *88*(1–2), 188–195. https://doi.org/10.1007/bf00371422

Turner, D. C. (1983). Upper Proterozoic schist belts in the Nigerian sector of the Pan-African province of West Africa. *Precambrian Research*, *21*(1–2), 55–79. https://doi.org/10.1016/0301-9268(83)90005-0

Ukwang, E. E., Ekwueme, B. N., & Kröner, A. (2012). Single zircon evaporation ages: Evidence for the Mesoproterozoic crust in the southeastern Nigerian basement complex. *Chinese Journal of Geochemistry*, *31*(1), 48–54. https://doi.org/10.1007/s11631-012-0548-4

Van de Flierdt, T., Goldstein, S. L., Hemming, S. R., Roy, M., Frank, M., & Halliday, A. N. (2007). Global neodymium–hafnium isotope systematics—Revisited. *Earth and Planetary Science Letters*, *259*(3–4), 432–441. https://doi.org/10.1016/j.epsl.2007.05.003

Vermeesch, P. (2013). Multi-sample comparison of detrital age distributions. *Chemical Geology*, *341*, 140–146. https://doi.org/10.1016/j.chemgeo.2013.01.010

Vermeesch, P. (2018). IsoplotR: A free and open toolbox for geochronology. *Geoscience Frontiers*, *9*(5), 1479–1493. https://doi.org/10.1016/j.gsf.2018.04.001

Vermeesch, P. (2021). On the treatment of discordant detrital zircon U–Pb data. *Geochronology*, *3*(1), 247–257. https://doi.org/10.5194/gchron-3-247-2021

Vermeesch, P., & Garzanti, E. (2015). Making geological sense of 'Big Data'in sedimentary provenance analysis. *Chemical Geology*, *409*, 20–27. https://doi.org/10.1016/j.chemgeo.2015.05.004

Vermeesch, P., Resentini, A., & Garzanti, E. (2016). An R package for statistical provenance analysis. *Sedimentary Geology*, *336*, 14–25. https://doi.org/10.1016/j.sedgeo.2016.01.009

Vermeesch, P., Rittner, M., Petrou, E., Omma, J., Mattinson, C., & Garzanti, E. (2017). High throughput petrochronology and sedimentary provenance analysis by automated phase mapping and LAICPMS. *Geochemistry, Geophysics, Geosystems*, *18*(11), 4096–4109. https://doi.org/10.1002/2017GC007109

Vervoort, J. D., Patchett, P. J., Blichert-Toft, J., & Albarède, F. (1999). Relationships between Lu–Hf and Sm–Nd isotopic systems in the global sedimentary system. *Earth and Planetary Science Letters*, *168*(1–2), 79–99. https://doi.org/10.1016/s0012-821x(99)00047-3

Vezzoli, G., Garzanti, E., Limonta, M., Andò, S., & Yang, S. (2016). Erosion patterns in the Changjiang (Yangtze River) catchment revealed by bulk-sample versus single-mineral provenance budgets. *Geomorphology*, *261*, 177–192. https://doi.org/10.1016/j.geomorph.2016.02.031

Vincent, V. I., Wang, L. X., Zhu, Y. X., Kamaunji, V. D., Ahmed, H. A., Ntekim, E. E., & Cao, L. (2022). Onset of the anorogenic alkaline magmatism in the Nigerian Younger Granite province: Constraints from the Daura and Dutse complexes. *Lithos*, *410*, 106561. https://doi.org/10.1016/j.lithos.2021.106561

von Eynatten, H., & Dunkl, I. (2012). Assessing the sediment factory: The role of single grain analysis. *Earth-Science Reviews*, *115*(1–2), 97–120. https://doi.org/10.1016/j.earscirev.2012.08.001

Wang, X., Griffin, W. L., & Chen, J. (2010). Hf contents and Zr/Hf ratios in granitic zircons. *Geochemical Journal*, *44*(1), 65–72. https://doi.org/10.2343/geochemj.1.0043

Welcomme, R. L., & Dumont, H. L. (1986). The Niger River system. In B. R. Davies, & K. F. Walker (Eds.), *The ecology of river systems* (Vol. 60, pp. 9–59). Springer, Monographiae Biologicae. https://doi.org/10.1007/978-94-017-3290-1_2

Wiedenbeck, M., Hanchar, J. M., Peck, W. H., Sylvester, P., Valley, J., Whitehouse, M., et al. (2004). Further characterisation of the 91500 zircon crystal. *Geostandards and Geoanalytical Research*, *28*(1), 9–39. https://doi.org/10.1111/j.1751-908x.2004.tb01041.x

Wu, F. Y., Liu, X. C., Ji, W. Q., Wang, J. M., & Yang, L. (2017). Highly fractionated granites: Recognition and research. *Science China Earth Sciences*, *60*(7), 1201–1219. https://doi.org/10.1007/s11430-016-5139-1

Yue, H., Gebremichael, M., & Nourani, V. (2022). Performance of the Global Forecast System's medium-range precipitation forecasts in the Niger River basin using multiple satellite-based products. *Hydrology and Earth System Sciences*, *26*(1), 167–181. https://doi.org/10.5194/hess-26-167-2022

Zaré, A., Mahé, G., Paturel, J. E., & Barbier, B. (2017). Influence du Bani sur la variabilité saisonnière et interannuelle de la crue du fleuve Niger dans le delta intérieur au Mali. *Hydrological Sciences Journal*, *62*(16), 2737–2752. https://doi.org/10.1080/02626667.2016.1148816

Zeh, A., & Holness, M. B. (2003). The effect of reaction overstep on garnet microtextures in metapelitic rocks of the Ilesha Schist Belt, SW Nigeria. *Journal of Petrology*, *44*(6), 967–994. https://doi.org/10.1093/petrology/44.6.967